Experimental Validation of Torsional Controllers for Drilling Systems

N. van de Wouw, T. Vromen, M. J. M. van Helmond, P. Astrid, A. Doris and H. Nijmeijer

Abstract Torsional stick-slip vibrations decrease the performance, reliability and fail-safety of drilling systems used for the exploration and harvesting of oil, gas, minerals and geo-thermal energy. Current industrial controllers regularly fail to eliminate stick-slip vibrations, especially when multiple torsional flexibility modes in the drill-string dynamics play a role in the onset of stick-slip vibrations. This chapter presents the experimental validation of novel robust output-feedback controllers designed to eliminate stick-slip vibrations in the presence of multiple dominant torsional

---

N. van de Wouw (✉) · H. Nijmeijer
The Department of Mechanical Engineering, Eindhoven University of Technology, Eindhoven, The Netherlands
e-mail: n.v.d.wouw@tue.nl

H. Nijmeijer
e-mail: h.nijmeijer@tue.nl

N. van de Wouw
Delft Center for Systems and Control, Delft University of Technology, Delft, The Netherlands

N. van de Wouw
The Department of Civil, Environmental & Geo-Engineering, University of Minnesota, Minneapolis, USA

T. Vromen
Océ Technologies B.V., Venlo, The Netherlands
e-mail: Thijs.vromen@oce.com

M. J. M. van Helmond
YER, Amsterdam, The Netherlands
e-mail: m.j.m.v.helmond@alumnus.tue.nl

P. Astrid
Shell Global Solutions International B.V., Rijswijk, The Netherlands
e-mail: patricia.astrid@shell.com

A. Doris
GeoSea nv, Geotechnical and Offshore Solutions, Zwijndrecht, Belgium
e-mail: doris.apostolos@deme-group.com

R. I. Leine et al. (eds.), *Advanced Topics in Nonsmooth Dynamics*,
https://doi.org/10.1007/978-3-319-75972-2_8

flexibility modes. For this purpose, a representative experimental test setup is designed, using a model of a real-life drilling rig as a basis. The model of the dynamics of the experimental setup can be cast in Lur'e-type form with set-valued nonlinearities representing an (uncertain) model for the complex bit-rock interaction and the interaction between the drill-string and the borehole. The proposed controller design strategy is based on skewed-μ-DK-iteration and aims at optimizing the robustness with respect to uncertainty in the non-smooth bit-rock interaction. Moreover, a closed-loop stability analysis for the non-smooth drill-string model is provided. Experimental results confirm that stick-slip vibrations are indeed eliminated using the designed controller in realistic drilling scenarios in which state-of-practice controllers have failed to achieve the same.

1 Introduction

Efficiency, reliability and safety are important aspects in the drilling of deep wells for the exploration and production of oil, gas, mineral resources and geo-thermal energy. Drill-strings several kilometers in length are used to transmit the axial force and torque necessary to drill the rock formations. These drill-string systems are known to exhibit different types of self-excited vibration, which decrease the drilling efficiency, accelerate bit wear, may cause sudden failure of expensive Measure-While-Drilling (MWD) tools, and may cause drill-string failure due to fatigue. This chapter focuses on the controlled mitigation of *torsional* stick-slip vibrations.

Modelling of the torsional dynamics of the drill-string is an important step towards the control of torsional vibrations. Most controller designs presented in literature rely on one- or two degree-of-freedom (DOF) models for the torsional dynamics only, see e.g., [4, 14, 31, 35]. The resisting torque-on-bit (TOB) is typically modelled as a frictional contact with a velocity weakening effect. Although experiments using single cutters to identify the bit-rock interaction law, see [5], do not reveal such a velocity weakening effect, analysis of models that take the coupled axial and torsional dynamics into account shows that such coupling effectively leads to a velocity weakening effect in the TOB [30]. This motivates a modelling-for-control approach that only involves the torsional dynamics and a set-valued, velocity weakening bit-rock interaction law. In contrast to other studies, however, we use a multi-modal model of the torsional dynamics, as field observations have revealed that multiple torsional resonance modes play a role in the onset of stick-slip oscillations.

Controllers for drilling systems aim to achieve drill-string rotation at a constant velocity and the mitigation of stick-slip vibrations. Moreover, the following control specifications are important. First, only surface measurements can be used for feedback. Second, the controller should be able to cope with dynamics related to multiple torsional flexibility modes. Third, robustness with respect to uncertainty in the non-smooth bit-rock interaction has to be guaranteed and, fourth control performance specifications, related to, e.g., measurement noise sensitivity and actuator constraints, need to be taken into account in the controller design.

A well-known control method, which aims at damping the first torsional mode, is the *Soft Torque Rotary system*, see [12]. The same objective is set in [14], which uses a PI-controller based on the top drive velocity. Other control methods have been developed, including torsional rectification [35], observer-based output-feedback [4, 6, 39], impedance matching [8], adaptive output-feedback for infinite dimensional drill-string models [1], weight-on-bit control [2] and robust control [15, 31]. Although important steps forward have been take in these works, an approach that satisfies all mentioned requirements has not yet been developed. A robust control approach, as proposed in [15, 31], is particularly suitable for this problem, since both robustness with respect to uncertainty of the system dynamics and control performance specifications can be taken into account in the control design. In [31], an $\mathscr{H}_\infty$ controller synthesis method is applied to a 2-DOF drill-string model and the twist in the drill-string is used as measurement, i.e., knowledge of the angular position of the bit is assumed. [15] uses the μ-synthesis technique through the DK-iteration procedure for the purpose of obtaining less conservative bounds on the uncertainty to obtain robustness with respect to the nonlinear bit-rock interaction. The model used is a similar 2-DOF model, and down-hole measurements (for assessing the twist of the drill-string) are also used in this case. Moreover, the employed 2-DOF models only take the first flexibility mode into account. In this chapter, we present experimental results of a robust control approach for the control of torsional drill-string vibrations, of which preliminary model-based results have been presented in [38] and which can cope with *multiple* torsional resonance modes.

Because of the high costs involved in testing on a real drilling rig, experimental lab-scale setups representing the drilling dynamics used for multiple purposes can be found in the literature, some examples of which are mentioned here (see [25] for a more comprehensive overview). In [22], an experimental 2-DOF drill-string system is used for the analysis of friction-induced stick-slip limit cycles. The same setup is used in [4] for experimental validation of an observer-based output-feedback controller. In [17], an experimental setup is developed that can emulate various excitation mechanisms of the drill-string, including stick-slip, well-borehole contact, and drilling fluid interaction. The aforementioned test setups both use brake systems to implement bit-rock interaction laws. A different approach is taken in [18], in which an experimental setup for exploring stick-slip phenomena is used that involves real cutting using a bit. In [36], an experimental setup is used to investigate whirling effects in drilling systems, involving both torsional and lateral dynamics. Another example of the experimental validation of a controller design approach to torsional vibrations in drilling systems can be found in [20]. Also for the testing of down-hole tools, experimental setups are used as a stepping stone towards implementation of the technique. For example, experimental results of Resonance Enhanced Drilling (RED) technology are presented in [40], and in [29], an experimental setup for investigating the Anti Stick-slip Tool (AST) is shown.

The need for a new experimental setup design stems from the fact that the controllers proposed in this thesis focus on the robustness with respect to multiple dominant torsional flexibility modes in the drill-string dynamics. To investigate this robustness, it is important that the experimental setup represents such a drilling system with multiple dominant flexibility modes (in contrast to, e.g., [22, 36], in which setups with a single flexibility mode are considered).

The main contributions of this chapter are, firstly, the model-based design of a representative (lab-scale) experimental drill-string setup, secondly, the design of a robust output-feedback controller methodology for eliminating stick-slip vibrations and, thirdly, experimental results showing the merit of the proposed control approach.

In Sect. 2, the design of the experimental setup is motivated and detailed. This design is based on a non-smooth model of a real drilling rig. Section 3 deals with the controller design strategy aiming to eliminate the torsional vibrations. In Sect. 4, the proposed control strategy is validated experimentally. The chapter closes with concluding remarks in Sect. 5.

2 Design of the Experimental Drill-String Setup

2.1 Model-Based Design of the Experimental Setup

Consider a drilling system, as schematically shown in Fig. 1. The investigated system is a realistic drill-string model of an offshore jack-up drilling rig, and the reservoir sections of the wells are drilled with a 6” PDC bit to reach depths of more than 6000 m along-hole and with an inclination angle up to 60°, resulting in significant resistive torques along the drill-string due to frictional borehole drill-string interaction. The rig is equipped with an AC top drive and fitted with a modern SoftTorque system [14, 19]. However, for this depth and hole size, stick-slip vibrations have been observed in

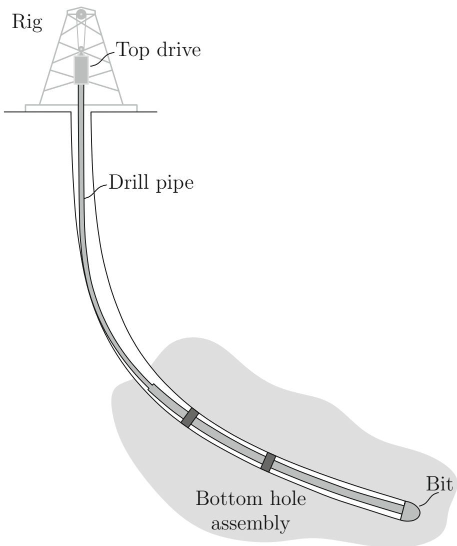

Fig. 1 Schematic drilling system, not to scale (adapted from [27])

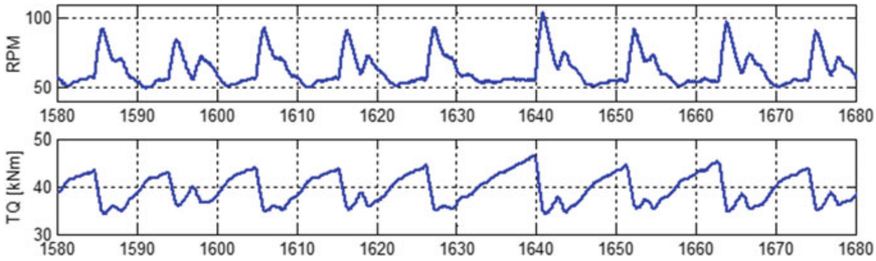

Fig. 2 Field data of the drilling rig under investigation, indicating severe stick-slip oscillations, see [11] (desired angular velocity is approximately 50 rpm). Top plot: top drive angular velocity in RPM; bottom plot: top drive torque

Fig. 3 Step-wise development of a model to be used as a basis for the design of the experimental setup

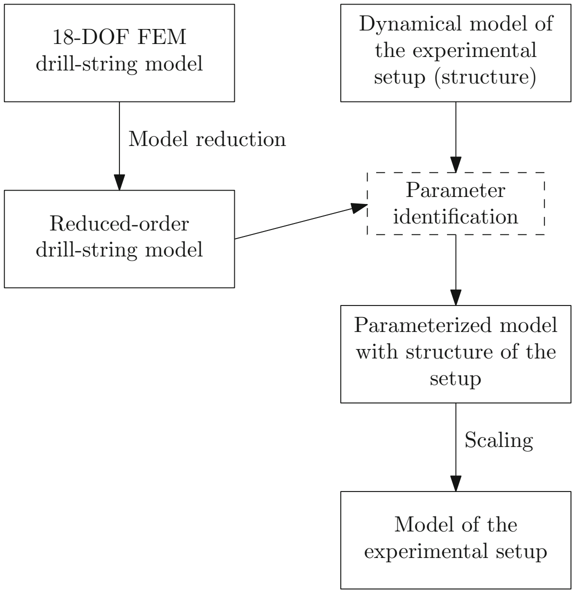

the field for this rig (see [11]), as shown in Fig. 2. In this figure, measurement data of the real rig is shown. The top drive angular velocity (RPM) and top drive torque (TQ) show severe oscillations, indicating stick-slip oscillations at the bit. The fact that a control strategy, which only damps the first flexibility mode of the torsional drill-string dynamics, fails to eliminate stick-slip vibrations shows that multiple resonance modes play a role and motivates construction of multi-modal drill-string models and development of a controller based on these models.

A finite-element method (FEM) model of this real-life drilling system is used as a basis for the design of the experimental drill-string setup. A detailed description of the FEM model is given in Sect. 2.1.1. Here, the focus is on the steps that are taken to develop a model of the experimental setup based on this 18-DOF FEM model. These steps are summarized in Fig. 3 and are discussed in more detail in the following sections. In Sect. 2.1.2, the model reduction strategy that is used for obtaining a reduced-order drill-string model is discussed. Next, the model of the experimental setup is explained in more detail in Sect. 2.1.3 and the identification approach for obtaining the parameters for this model based on the reduced-order model is given in Sect. 2.1.4. Since it is impossible to scale down an oil-field drill-string to a lab-scale setup that still exhibits the main (torsional) dynamics we aim to study, we propose a model with four rotating discs, coupled with (steel) strings, as shown in Fig. 4. It is important to mention that the proposed model of the experimental setup has a specific structure, due to the mechanical elements (i.e., inertias and springs) that are used in the setup resulting in a lumped-parameter model, while on the other hand, the reduced-order drill-string model does not have such a specific structure. The identified parameters of the obtained model are still of the same order of magnitude as the original drill-string model (e.g., inertia and stiffness properties of the system as a whole are still of the same order of magnitude, and are hence not (yet) scaled). As a consequence, the representative torsional velocity and torque levels of the setup match those of a real drill-string system. Therefore, scaling is used to obtain suitable torque levels and velocities for a lab-scale drill-string setup, but also to obtain feasible inertias and stiffnesses for the lab-scale experimental system design. This scaling procedure is discussed in Sect. 2.1.5.

2.1.1 Finite-Element Model

A finite-element model of this drilling system, which represents a drill-string 6249 m in length, has been developed, and the simulation results of this model have been validated with field data for a range of operational conditions (such as weight-on-bit (WOB) and angular velocity). The 18-DOF finite-element model is obtained by representing the drill-string with a number of equivalent pipe sections in order to accurately describe the torsional dynamics relevant to stick-slip vibrations. The model is validated by comparing the simulations of the non-smooth model (i.e., including bit-rock and borehole-drillstring interaction torques) with field measurements of the drill-string system. Figures 5 and 6 show two cases of this validation study, i.e., the simulation results of the finite-element model are compared with the field data under two different operating conditions; in both cases, the drill-string system exhibited stick-slip vibrations at the bit. As can be seen from these figures, the simulation results match the field data, both in terms of the amplitude and the frequency of the oscillations. The latter observations further motivate the usage of the developed model as a basis for controller design in this thesis.

Fig. 4 Schematic representation of a model with four discs

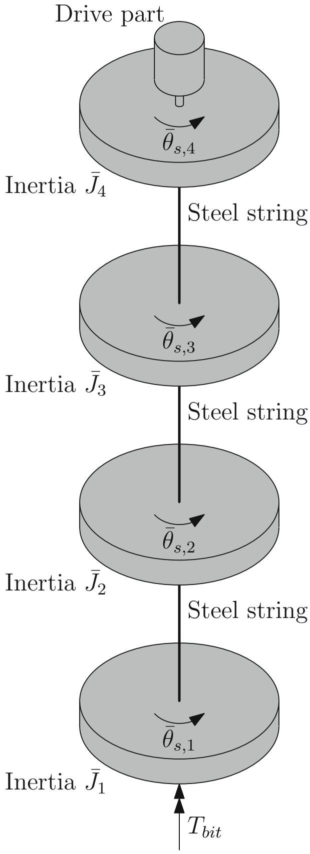

The finite-element method (FEM) representation of the drill-string is a model with 18 elements. The element at the top is a rotational inertia to model the top drive inertia, and the subsequent elements are equivalent pipe sections based on the dimensions and material properties of the drill-string (see [37] for more details). The resulting model can be written as a second-order differential equation of the following form:

$$M\ddot{\theta} + D\dot{\theta} + K_t\theta_d = S_w T_w(\dot{\theta}) + S_b T_{bit}(\dot{\theta}_1) + S_t T_{td} \tag{1}$$

with the rotational displacement coordinates $\theta \in \mathbb{R}^m$ with $m = 18$, the top drive motor torque input $T_{td} \in \mathbb{R}$ being the control input, the bit-rock interaction torque $T_{bit} \in \mathbb{R}$ and the interaction torques $T_w \in \mathbb{R}^{m-1}$ between the borehole and the drill-string acting on the nodes of the FEM model. The coordinates $\theta = \begin{bmatrix}\theta_1 \cdots \theta_m\end{bmatrix}^\top$ represent the angular displacements of the nodes of the finite-element representation. Next, we define the difference in angular position between adjacent nodes as

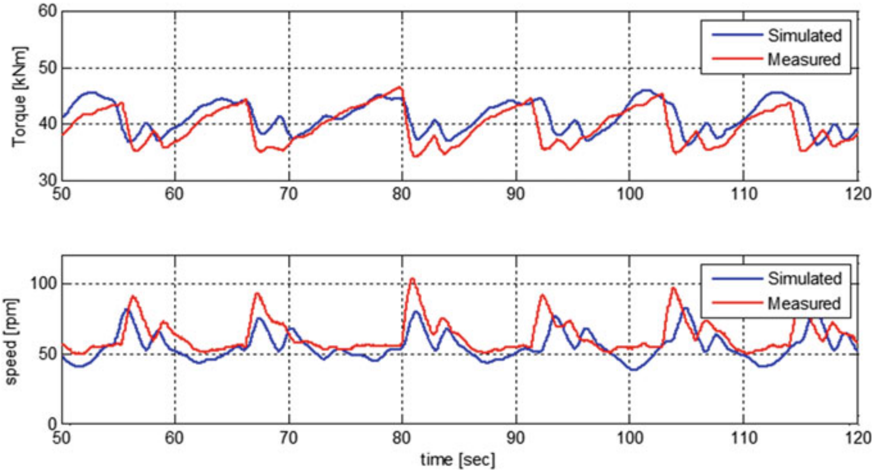

Fig. 5 Comparison between a simulation result of the FEM model and actual field data from the rig (top plot: top drive torque; bottom plot: top drive velocity); the desired angular velocity is approximately 50 rpm [11]

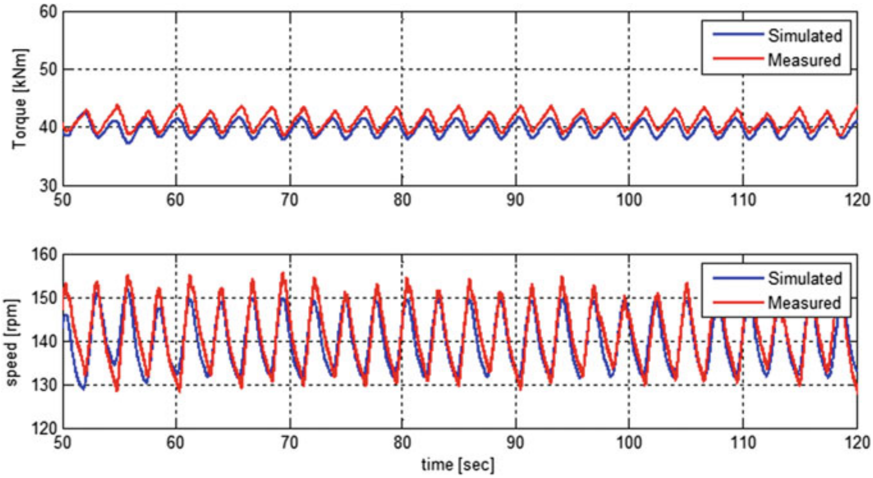

Fig. 6 Comparison between a simulation result of the FEM model and actual field data from the rig (top plot: top drive torque; bottom plot: top drive velocity); the desired angular velocity is approximately 140 rpm, [11]

follows: $\theta_d := \left[\theta_1 - \theta_2 \ \theta_2 - \theta_3 \ \cdots \ \theta_{m-1} - \theta_m\right]^\top$. In (1), the mass, damping and stiffness matrices are, respectively, given by $M \in \mathbb{R}^{m\times m}$, $D \in \mathbb{R}^{m\times m}$ and $K_t \in \mathbb{R}^{m\times m-1}$, and the matrices $S_w \in \mathbb{R}^{m\times m-1}$, $S_b \in \mathbb{R}^{m\times 1}$ and $S_t \in \mathbb{R}^{m\times 1}$ represent the generalized force directions of the interaction torques, the bit torque and the input torque, respectively. The coordinates θ are chosen such that the first element (θ_1) describes

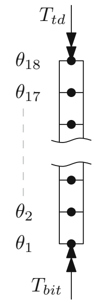

Fig. 7 Schematic representation of the 18-DOF finite-element model

the rotation of the bit and the last element (θ_{18}) the rotation of the top drive at the surface, as illustrated in Fig. 7. The interaction between the borehole and the drill-string is modelled as (set-valued) Coulomb friction, that is,

$$T_{w,i} \in T_i \text{ Sign}\left(\dot{\theta}_i\right), \quad \text{for } i = 2, \ldots, m, \tag{2}$$

with T_i representing the amount of friction at each element and the set-valued sign function defined as

$$\text{Sign}(y) := \begin{cases} -1, & y < 0 \\ [-1, 1], & y = 0 \\ 1, & y > 0. \end{cases} \tag{3}$$

Note that possible viscous effects between the drill-string and the borehole are captured in the damping matrix D, which motivates only Coulomb effects being taken into account in the interaction torques T_w. The set-valued bit-rock interaction model is given by

$$T_{bit}(\dot{\theta}_1) \in \text{Sign}\left(\dot{\theta}_1\right)\left(T_d + (T_s - T_d)\, e^{-v_d|\dot{\theta}_1|}\right), \tag{4}$$

where T_s is the static torque, T_d the dynamic torque and $v_d := \frac{30}{N_d \pi}$ s/rad indicates the decrease from static to dynamic torque. A schematic representation of the bit-rock interaction is shown in Fig. 8. For typical parameter settings, the ratio between T_s and T_d is within the range 2–5, i.e., the static torque is 2 to 5 times higher than the dynamic torque. Moreover, typical parameter settings for N_d are such that the decrease from static to dynamic torque is mainly between 0 and 20–30 rpm, which results in a severe velocity-weakening effect in the bit-rock interaction for low angular velocities.

2.1.2 Reduced-Order Model

The FEM model presented above has 18 degrees of freedom. For the design of the setup, we rely on a reduced-order model. The purpose of this reduced-order model is to approximate the higher-order FEM model with a reduced number of states, while

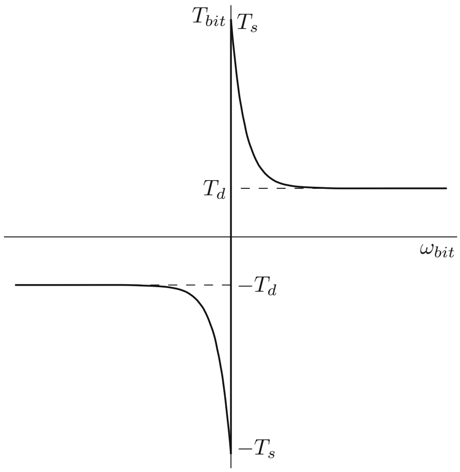

Fig. 8 Schematic representation of the bit-rock interaction T_{bit} in (4); $\omega_{bit} := \dot{\theta}_1$

still preserving the key dynamic system properties. As mentioned before, models with multiple flexibility modes are considered, because field observations have revealed that higher flexibility modes of the drill-string also play a role in the onset of stick-slip vibrations (see [23]). As mentioned in [37], the first three resonance modes, with resonance frequencies at $f_1 \approx 0.15$, $f_2 \approx 0.38$ and $f_3 \approx 0.53$ Hz, are dominant in the drill-string dynamics (see Figs. 9, 10 and 11). Therefore, a drill-string model with at least four degrees of freedom is considered capable of enabling the accurate capture of those first three flexibility modes and the rigid body mode by the reduced-order model.

For the design of the experimental setup, we aim to accurately approximate the torsional flexibility modes of the drill-string system associated with the lowest resonance frequencies. Therefore, an eigenmode-based reduction strategy is used, also known as the mode displacement method [10]. Now, let us consider the undamped (and unforced) drill-string system and, in addition, the stiffness matrix K related to the absolute angular positions $\theta = \begin{bmatrix}\theta_1 & \cdots & \theta_m\end{bmatrix}^\top$, instead of the stiffness matrix K_t, related to the difference in angular position θ_d as in (1), hence $M\ddot{\theta} + K\theta = 0$. Then, the mode displacement method is based on the free vibration modes of these structural dynamics. This leads to the following generalized eigenvalue problem: $\left[K - \lambda_i^2 M\right] v_i = 0$, where v_i is the mode shape vector corresponding to the eigenfrequency λ_i, with $i \in [1, \ldots, m]$. The resulting eigenfrequencies are grouped in ascending order, i.e., $\lambda_1 \leq \lambda_2 \leq \cdots \leq \lambda_m$, and the corresponding eigenmodes $v_1, v_2, \ldots, v_m$ are collected in the square $(m \times m)$ modal matrix $V = \begin{bmatrix}v_1 & v_2 & \cdots & v_m\end{bmatrix}$. Using this matrix, we employ the following coordinate transformation to modal coordinates η:

$$\theta = V\eta. \tag{5}$$

The general idea of the reduction approach is to keep the first $m_r < m$ eigenvectors, which correspond to the lowest eigenfrequencies in the reduced-order model. Hereto, consider the following transformation matrix $T = \begin{bmatrix} v_1 & v_2 & \cdots & v_{m_r} \end{bmatrix}$. Using this transformation matrix, (5) can be rewritten as

$$\theta = \begin{bmatrix} T & U \end{bmatrix} \begin{bmatrix} \theta_r \\ \eta_2 \end{bmatrix} = T\theta_r + U\eta_2, \tag{6}$$

where U contains the truncated eigenmodes, that is, the eigencolumns $m_r + 1$ to m, and η_2 contains the states that correspond to these modes; the coordinates preserved in the reduced-order model are denoted by θ_r. Using (1) and (6) and projecting the resulting equations of motion on the expansion basis T results in the following reduced-order dynamics:

$$M_r\ddot{\theta}_r + D_r\dot{\theta}_r + K_r\theta_r = T^\top S_w T_w(\dot{\check{\theta}}) + T^\top S_b T_{bit}(\dot{\check{\theta}}_1) + T^\top S_t T_{td} \tag{7}$$

with $M_r = T^\top MT \in \mathbb{R}^{m_r \times m_r}$, $D_r = T^\top DT \in \mathbb{R}^{m_r \times m_r}$, $K_r = T^\top KT \in \mathbb{R}^{m_r \times m_r}$ and $\check{\theta} := T\theta_r \in \mathbb{R}^m$ being the estimated (full-order) angular displacements based on the reduced-order estimates.

In this work, the case in which $m_r = 4$ is considered, that is, we take the rigid body mode and three torsional flexibility modes into account. The relevant frequency response functions of the (linear) drill-string dynamics are shown in Figs. 9, 10 and 11. These frequency response functions describe the (linear) drill-string dynam-

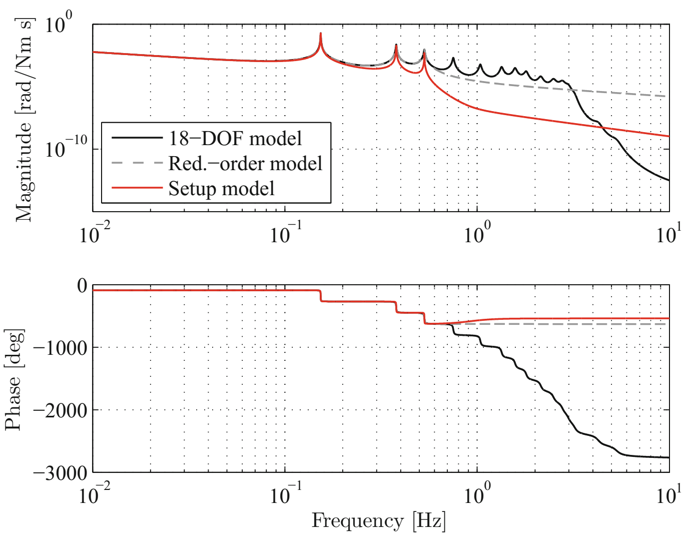

Fig. 9 Frequency response function of the 18-DOF model, the reduced-order model and the setup model with the identified parameters from input torque T_{td} to bit velocity ω_{bit}

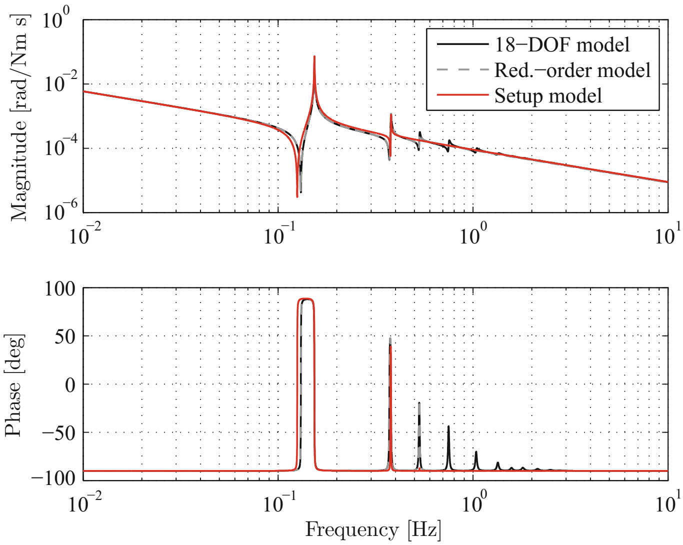

Fig. 10 Frequency response function of the 18-DOF, the reduced-order model and the setup model with the identified parameters from input torque T_{td} to top drive velocity ω_{td}

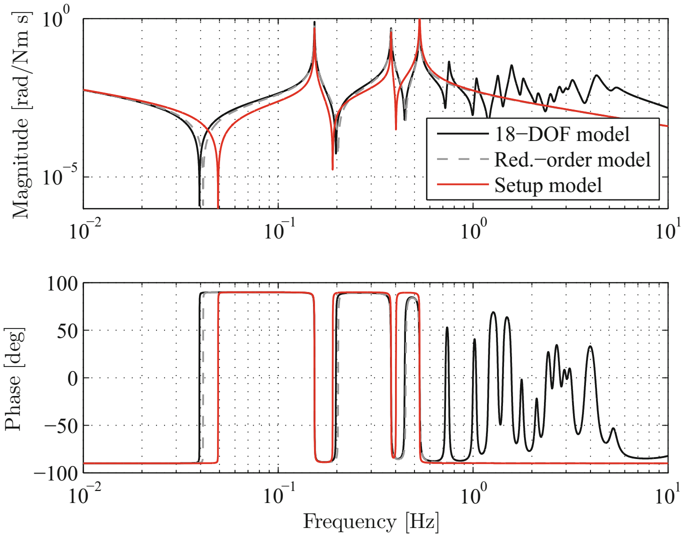

Fig. 11 Frequency response function of the 18-DOF, the reduced-order model and the setup model with the identified parameters from bit torque T_{bit} to bit velocity ω_{bit}, i.e., bit-mobility

ics from the relevant inputs (top drive torque and bit-rock interaction torque) to the angular velocity outputs at the top drive and bit, i.e., respectively, $\omega_{td} := \dot{\theta}_{18}$ and $\omega_{bit} := \dot{\theta}_1$. As can be observed, the first three eigenmodes are indeed accurately matched by the reduced-order model.

2.1.3 Dynamical Model of the Experimental Setup

In this section, the model that is used for the design of the experimental setup, as shown in Fig. 4, is discussed in more detail. For the model, we will not restrict ourselves to connections between adjacent discs, but will also take potential connections between all the discs into account. The coordinates $\bar{\theta}_s = \left[\bar{\theta}_{s,1} \cdots \bar{\theta}_{s,4}\right]^\top$ represent the angular displacements of the discs. The equations of motion of the system are given by:

$$\bar{M}_s\ddot{\bar{\theta}}_s + \bar{D}_s\dot{\bar{\theta}}_s + \bar{K}_s\bar{\theta}_s = S_{ws}T_{ws}(\dot{\bar{\theta}}_s) + S_{bs}T_{bit}(\dot{\bar{\theta}}_{s,1}) + S_{ts}T_{td}, \tag{8}$$

with

$$\bar{M}_s = \begin{bmatrix} \bar{J}_1 & 0 & 0 & 0 \\ 0 & \bar{J}_2 & 0 & 0 \\ 0 & 0 & \bar{J}_3 & 0 \\ 0 & 0 & 0 & \bar{J}_4 \end{bmatrix} \tag{9}$$

$$\bar{D}_s = \begin{bmatrix} \bar{d}_{12}+\bar{d}_{13}+\bar{d}_{14} & -\bar{d}_{12} & -\bar{d}_{13} & -\bar{d}_{14} \\ -\bar{d}_{12} & \bar{d}_{12}+\bar{d}_{23}+\bar{d}_{24} & -\bar{d}_{23} & -\bar{d}_{24} \\ -\bar{d}_{13} & -\bar{d}_{23} & \bar{d}_{13}+\bar{d}_{23}+\bar{d}_{34} & -\bar{d}_{34} \\ -\bar{d}_{14} & -\bar{d}_{24} & -\bar{d}_{34} & \bar{d}_{14}+\bar{d}_{24}+\bar{d}_{34} \end{bmatrix}, \tag{10}$$

$$\bar{K}_s = \begin{bmatrix} \bar{k}_{12}+\bar{k}_{13}+\bar{k}_{14} & -\bar{k}_{12} & -\bar{k}_{13} & -\bar{k}_{14} \\ -\bar{k}_{12} & \bar{k}_{12}+\bar{k}_{23}+\bar{k}_{24} & -\bar{k}_{23} & -\bar{k}_{24} \\ -\bar{k}_{13} & -\bar{k}_{23} & \bar{k}_{13}+\bar{k}_{23}+\bar{k}_{34} & -\bar{k}_{34} \\ -\bar{k}_{14} & -\bar{k}_{24} & -\bar{k}_{34} & \bar{k}_{14}+\bar{k}_{24}+\bar{k}_{34} \end{bmatrix}, \tag{11}$$

$$S_{ws} = \begin{bmatrix} 0&0&0 \\ 1&0&0 \\ 0&1&0 \\ 0&0&1 \end{bmatrix}, \quad S_{bs} = \begin{bmatrix} 1 \\ 0 \\ 0 \\ 0 \end{bmatrix}, \quad S_{ts} = \begin{bmatrix} 0 \\ 0 \\ 0 \\ 1 \end{bmatrix}, \tag{12}$$

and the resistive torques at discs 2, 3 and 4 for modeling the borehole drill-string interaction are given by T_{ws}. Recall that T_{td} denotes the top drive motor torque and T_{bit} denotes the bit-rock interaction torque.

2.1.4 Parameter Identification for the Setup Model

The next step is to determine the parameters of the 4-DOF model of the experimental setup based on the reduced-order model presented in Sect. 2.1.2. First, the inertias of the four discs are determined. The total inertia of the 4-disc setup is chosen to be equal to the total inertia of the original 18-DOF model. In addition, we require the inertia of the upper disc ($\bar{J}_4$) to be equal to the inertia of the top drive, such that the upper disc actually represents the top drive. Doing so, the torque in the drill-string below disc 4 comes to represent the pipe torque that is used as measurement in the linear robust controller approach (presented in Sect. 3). The inertia of the bottom disc ($\bar{J}_1$) is determined based on the "high"-frequency behavior (i.e., above the eigenfrequencies) of the reduced-order model. The remaining part of the total inertia is equally distributed over the two remaining discs. The remaining damping and stiffness parameters, are determined using an optimization-based identification approach. The objective of the optimization procedure is to find the model parameters such that the difference in the complex plane between the frequency response function of the reduced-order model and the model of the setup is minimized over all frequencies within the frequency range of interest. Hence, we seek to solve the following optimization problem:

$$\min_{p \in \left[\underline{p},\, \overline{p}\right]} J(p), \tag{13}$$

where $p := \left[\bar{k}_{12}\ \bar{k}_{23}\ \bar{k}_{34}\ \bar{k}_{13}\ \bar{k}_{14}\ \bar{k}_{24}\ \bar{d}_{12}\ \bar{d}_{23}\ \bar{d}_{34}\ \bar{d}_{13}\ \bar{d}_{14}\ \bar{d}_{24}\right]$ are the parameters of the setup to be determined, $\underline{p}$ and $\overline{p}$, represent a lower and upper bound for the parameters and the objective function $J(p)$ is given by

$$J(p) = \sum_{\omega_l} w(j\omega) \left(\left| W(j\omega) H_r^{T_{td}\omega_{bit}}(j\omega) - W(j\omega) H_s^{T_{td}\omega_{bit}}(j\omega) \right|^2 \right) \tag{14}$$

with $H_r^{T_{td}\omega_{bit}}$ and $H_s^{T_{td}\omega_{bit}}$ the frequency response functions from top drive torque input to bit velocity output of the reduced-order model and the setup model, respectively. The frequency response function from top drive torque input to bit velocity output is chosen for the parameter identification because it captures the relevant dynamics of the drilling system that should be represented in the setup. Note that $H_s^{T_{td}\omega_{bit}}$ depends on the parameters p. The frequency grid ω_l is a discrete grid of frequencies between 0.05 and 6 Hz, because that is the relevant frequency range of the reduced-order drill-string dynamics (see Fig. 9). The frequency-dependent weighting filter $W(j\omega)$ is chosen to be $W(j\omega) = J_{tot}\, j\omega$, to compensate for the negative slope of the frequency response function from top drive torque input to bit velocity output. The (scalar) multiplication factor $w(j\omega)$ in (14) is used to give extra weighting in specific frequency ranges. This multiplication factor is equal to 1.5 for $0.14 < f < 0.165$ (i.e., around the first resonance frequency), equal to 2 for $0.5 < f < 0.57$ (i.e., around the third resonance frequency) and equal to 1 for all other frequencies.

The results of the fitting procedure are shown in Figs. 9, 10 and 11. Note that the identified parameters are still of the same order of magnitude as for the original drill-string model. For example, the inertia of the upper disc is equal to the inertia of a real top drive (approximately 1800 kgm^2) and a driving torque at the top drive is typically on the order of 40 kNm. These settings are infeasible for a lab-scale setup. Therefore, scaling of the parameters in order to obtain feasible dimensions for the lab-scale setup is discussed in Sect. 2.1.5. It turned out that it is not possible to fit the reduced-order model of the original drill-string and the model of the setup. This is mainly caused by the fact that in the finite-element model (and therefore also in the reduced-order model), the drill-string's properties are distributed along it, whereas the model of the setup is based on a lumped mass approach (multiple discs representing discrete inertias). This is particularly visible in Fig. 9: due to the lumped inertias of the setup model, the slope of the magnitude of the FRF decreases by 2 (on a loglog-scale) after each resonance peak and the phase decreases by 180 degrees (due to the 2 poles associated with the resonance). However, the FRFs of the 18-DOF and reduced-order model do not show this behavior; this is caused by zeros of these models that are in the right-half-plane of the complex plane (i.e., non-minimum phase). Nevertheless, a satisfactory match of the dominant resonances is achieved and, moreover, simulation results of the non-smooth setup model (see Fig. 12) confirm that the response of the setup model is in good correspondence with the response of the reduced-order model and the original 18-DOF FEM model. In Fig. 12, the response of the 18-DOF drill-string model is compared with the response of the 4-DOF setup model. In both simulations, the system is controlled with a SoftTorque controller (see (37) in Sect. 4.2) and the parameters $c_t = 1829$ and $k_t = 1177$), and the desired angular velocity is equal to 50 rpm. Clearly, the response of the setup model is similar to the response of the original FEM model. This illustrates that the dominant dynamics of the original 18-DOF model is captured by the 4-DOF setup model, also in the scope of the non-smooth dynamics leading to stick-slip oscillations.

2.1.5 Scaling of the Drill-String Model

An identified set of parameters for the experimental setup has been obtained in the previous section. However, these parameters are based on a full-scale drilling rig and, as mentioned before, such parameter values are infeasible for a lab-scale experimental setup. To obtain feasible parameter values for the experimental setup, a scaling of the variables and parameters is in order, while retaining the resonance frequencies of the drill-string system. Therefore, two scaling factors are introduced: c_1 is used to scale the torque level and c_2 to scale the states of the system. The states are scaled according to $\theta_s = \frac{1}{c_2}\bar{\theta}_s$ and the equations of motion are pre-multiplied with a factor $\frac{1}{c_1}$ to scale the torque level. This results in the (scaled) equations of motion given by

$$M_s\ddot{\theta}_s + D_s\dot{\theta}_s + K_s\theta_s = S_{ws}\hat{T}_{ws}(\dot{\theta}_s) + S_{bs}\hat{T}_{bit}(\dot{\theta}_{s,1}) + S_{ts}\hat{T}_{td} \tag{15}$$

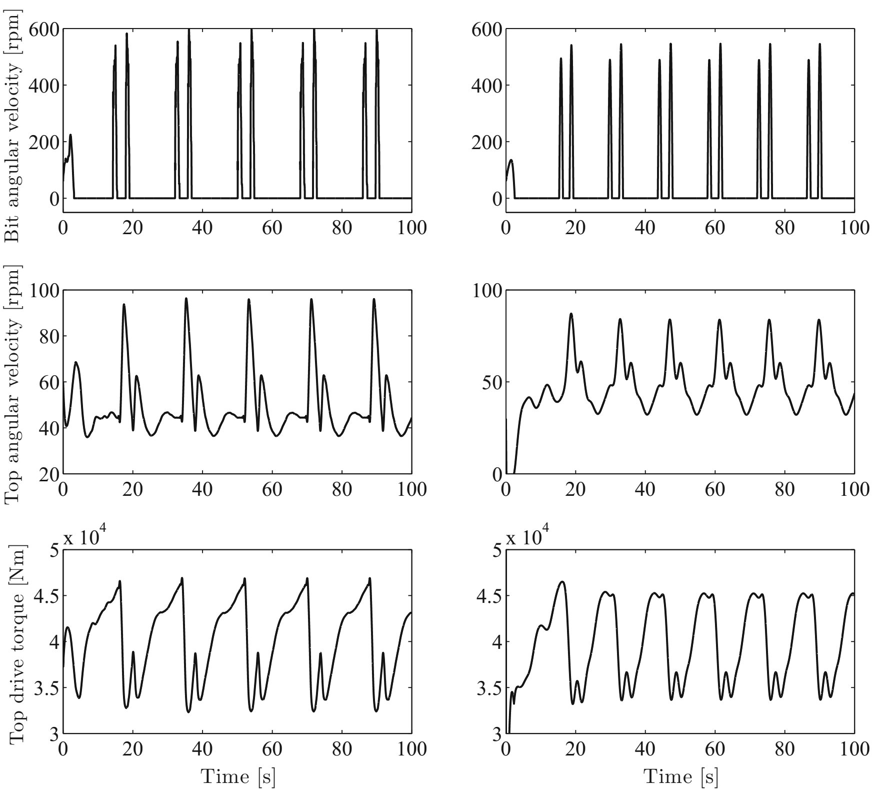

Fig. 12 Simulation result of the 18-DOF drill-string model (left-hand side) compared with a simulation result of the 4-DOF model of the experimental setup (right-hand side)

with $M_s := \frac{c_2}{c_1}\bar{M}_s$, $D_s := \frac{c_2}{c_1}\bar{D}_s$, $K_s := \frac{c_2}{c_1}\bar{K}_s$, $\hat{T}_{ws} := \frac{1}{c_1}T_{ws}$, $\hat{T}_{bit} := \frac{1}{c_1}T_{bit}$ and $\hat{T}_{td} := \frac{1}{c_1}T_{td}$. The scaled bit-rock interaction torque $\hat{T}_{bit}$ is given by the following scaled law:

$$\hat{T}_{bit}(\dot{\theta}_{s,1}) \in \text{Sign}\left(\dot{\theta}_{s,1}\right)\left(\hat{T}_d + \left(\hat{T}_s - \hat{T}_d\right)e^{\left(-30\,|\dot{\theta}_{s,1}|\right)/\left(\hat{N}_d\pi\right)}\right) \tag{16}$$

with $\hat{T}_d = \frac{1}{c_1}T_d$, $\hat{T}_s = \frac{1}{c_1}T_s$ and $\hat{N}_d = \frac{1}{c_2}N_d$, and the scaled drill-string borehole interaction torques can be written as

$$\hat{T}_{ws,i} \in \hat{T}_{s,i}\ \text{Sign}\left(\dot{\theta}_{s,i}\right), \quad \text{for } i = 2, \ldots, m, \tag{17}$$

where $\hat{T}_{s,i} = \frac{1}{c_1}T_{s,i}$. The scaling factors are determined to be $c_1 = 6250$ and $c_2 = 10$. This scaling is chosen first, to obtain feasible torque levels for typical motors that can be used in lab-scale systems (mainly influenced by c_1) and, second, to achieve angular position differences between adjacent discs that are sufficiently small so as to avoid plastic deformation of the steel strings between those discs. The latter aspect, of course, also depends on the length and diameter of the strings, which need to have feasible dimensions. The scaled parameters are summarized in Table 1, the scaled parameters regarding the interaction torques are given in Table 2. The top drive torque is on the order of 40 kNm for the full scale system, whereas this is scaled to approximately 6.4 Nm for the setup, and since the states are scaled with a factor 10, a desired angular velocity of 50 rpm in practice is equal to a desired angular velocity of 5 rpm in the setup. Note that no time-scaling applied, which implies that the resonance frequencies of the system have not been changed.

By applying the described scaling, the model of the experimental drill-string setup is scaled to feasible dimensions for designing a lab-scale setup. With the method described in this section, a set of prescribed model parameters is obtained for the design of the setup. The setup design is discussed in more detail in the next section.

2.2 The Experimental Drill-String Setup

The experimental setup is designed to be adjustable and modular. In particular, it is designed such that it should be possible to change the inertia of the discs and the stiffness of the strings, and, by using a hardware-in-the-loop approach, other parameters such as damping can also be adjusted. With this hardware-in-the-loop approach, additional dynamics is emulated in software and implemented using motors driving all the individual discs. In addition, the setup is designed such that it is possible to

Table 1 Parameters of the setup model

Symbol	Value (kgm^2)	Symbol	Value (Nms/rad)	Symbol	Value (Nm/rad)
J_1	0.064	k_{12}	0.630	d_{12}	0
J_2	0.708	k_{23}	1.799	d_{23}	0.0018
J_3	0.708	k_{34}	1.097	d_{34}	0.0024
J_4	2.845	k_{13}	0	d_{13}	0
		k_{14}	0	d_{14}	0.0005
		k_{24}	0	d_{24}	0

Table 2 Parameters of the scaled bit-rock interaction model and drill-string borehole interaction torques

Symbol	Value	Symbol	Value (Nm)
$\hat{T}_s$	1.232 Nm	$\hat{T}_{s,2}$	2.297
$\hat{T}_d$	0.272 Nm	$\hat{T}_{s,3}$	3.038
$\hat{N}_d$	0.5 rad/s	$\hat{T}_{s,4}$	0.662

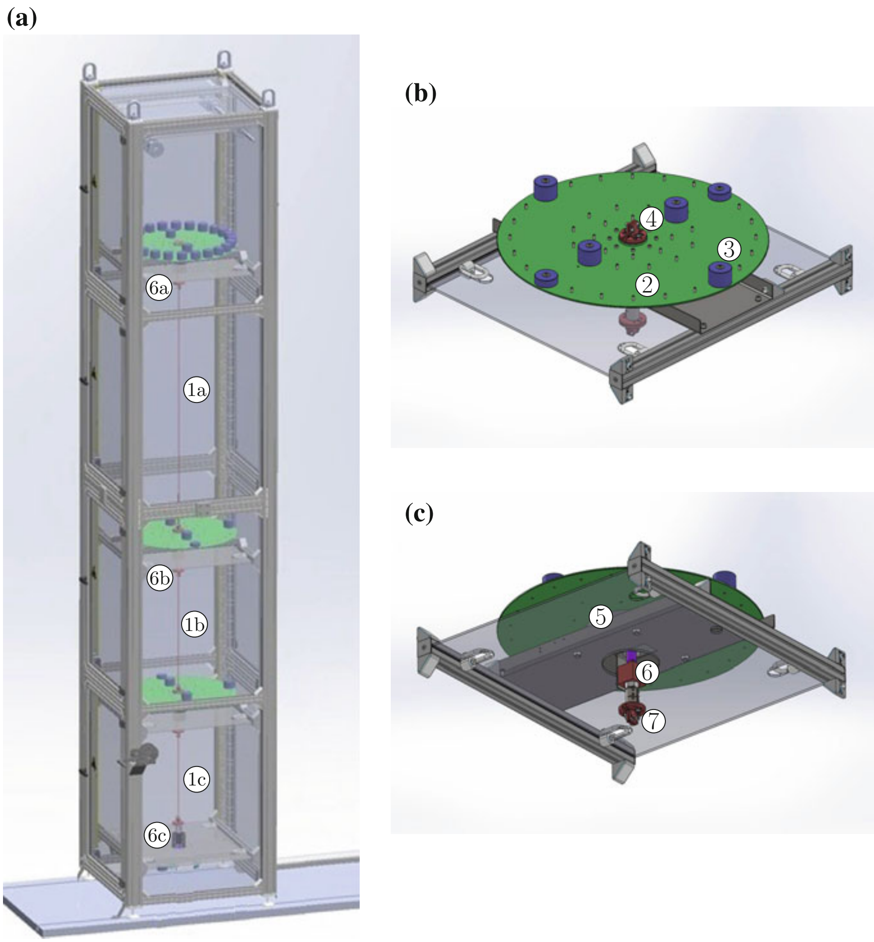

Fig. 13 Schematic representation of the experimental drill-string setup. **a** is an overview of the setup, **b** is a top view on one of the disc platforms, **c** is a bottom view of one of the disc platforms. Different parts are numbered as follows: 1- (steel) strings between the different discs; 2- disc (representing inertia); 3- additional masses to change the inertia of the disc; 4- upward connection for the string; 5- flat hollow shaft torque motor (embedded in the frame); 6- torque sensors; 7- downward connection for the string

investigate a system with additional flexibility modes by adding an extra disc to the setup. A schematic overview of the setup is shown in Fig. 13.

Let us now discuss the design of the setup in more detail. The total setup is 5 m tall and has a footprint of 1×1 m. As can be seen in Fig. 13a, the setup has 4 disc platforms to support the 4 discs of the model (see Fig. 13b, c; note that the bottom disc platform is slightly different, which is explained in more detail later). These discs are interconnected by steel strings to represent the torsional stiffness of the drill-string system and each disc is equipped with a motor. For the top disc, this motor is used to drive the system and to apply the desired control action. At the bottom disc, the motor is used to emulate the desired bit-rock interaction, and at the intermediate discs, the drill-string borehole interaction torques are implemented using these motors. In addition, these motors are used to emulate the hardware-in-the-loop components, such as damping torque associated with the damping constant d_{14}, and to compensate for undesired effects, such as friction and cogging in the motors. Each of the motors is equipped with an encoder, and the setup contains three torque sensors for measuring the torques in the interconnecting strings. Furthermore, a DS1103 controller board from dSPACE [7] is used as a real-time control and data acquisition platform. A photo of the lab-scale drill-string system is shown in Fig. 14.

The three upper disc platforms are identical and equipped with Georgii Kobold KTY-F torque motors ([9]). These are flat direct-drive brushless DC motors with a maximum torque of 26 Nm and a maximum angular velocity of 250 rpm. To actuate and control these motors, Siep & Meyer SD2S motor amplifiers ([33]) are used, and to measure the angular position of the discs, built-in 19-bit Heidenhain ECI 119 inductive encoders ([13]) are used. The 19-bit encoder signal is converted, in the motor amplifiers, into a 15-bit quadrature signal that is used by the dSPACE system to determine the angular position of the discs. The angular velocities of the discs are determined by numerical differentiation of the angular positions measured by the encoders. The discs have an inertia of approximately 0.350 kgm^2, including the inertia of the motor. By adding additional masses at a certain radius on the discs, the inertia of the discs can be adjusted (in steps of approximately 0.05 kgm^2) to obtain the desired inertia, as specified in Table 1.

The bottom disc platform is shown in Fig. 15 and is different from the other platforms. This difference has two main reasons: first, the specified inertia of the bottom disc is much lower compared to the inertias of the other discs and, second, in order to accurately implement the desired bit-rock interaction law, it is important that this disc has a low static friction. To realize these two aspects, a disc with a smaller diameter and a different type of motor is used. The installed motor is a brushed DC motor from Printed Motor Works (type: GN16RE), see [28], with a maximum torque of 2.55 Nm and a maximum angular velocity of 3000 rpm. The static friction in this motor is approximately 0.05 Nm, which is sufficiently lower than the dynamic torque level $\hat{T}_d$ to be implemented (see Table 2). In addition, a 16-bit Sick DFS60A incremental encoder ([32]) is used together with a Copley Controls Xenus Plus motor amplifier (type: XTL-230-40), see [3]. The bottom disc has an inertia of approximately 0.03 kgm^2 and can be adjusted in steps of approximately 0.01 kgm^2 to achieve the prescribed inertia.

To represent the torsional stiffness of the drill-string model, steel strings with a specific length and diameter are used. The length and diameter are chosen such that the prescribed stiffnesses (see Table 1) are achieved. The specified damping factors are obtained by implementing the damping using the motors (i.e., in a hardware-in-the-loop fashion) based on the measured difference in angular velocity of the discs, while compensating for the material damping that is already present in the strings.

Fig. 14 The experimental drill-string setup

The setup is also equipped with three PCM TQ-RT2A-25NM torque sensors [26]. These sensors can measure up to 25 Nm with an accuracy of ±0.2%. The torque sensors are placed below the upper two discs and just above the bottom disc, as indicated in Figure 13a with 6a-c. The torque sensor below the top drive disc will be used for the pipe torque measurement, to be used in the scope of feedback control.

The foregoing description of the experimental setup shows that the setup is equipped with multiple sensors: encoders in all the discs to measure the angular

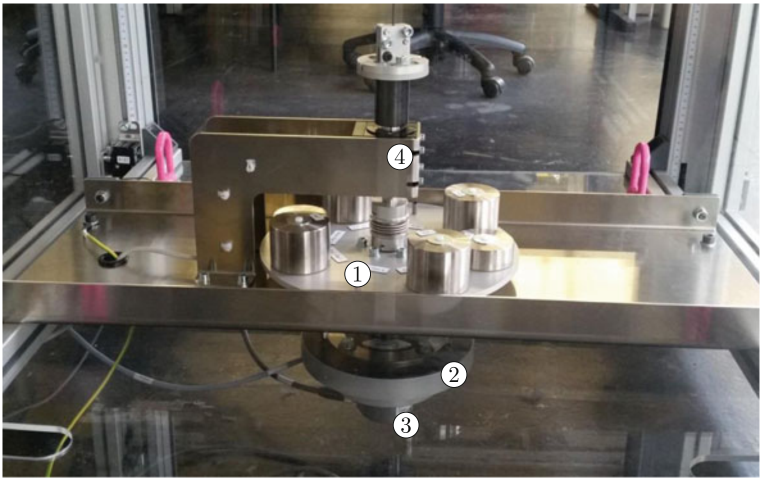

Fig. 15 Bottom disc platform, with 1: the disc with additional weights; 2: the motor; 3: the encoder; 4: the torque sensor

position (and determine the angular velocity) and three torque sensors to measure the torques in the steel strings between the discs. However, the control design strategies to be presented in later sections will only require surface (top-side) measurements. The extra sensors, which are not required for the proposed control strategies, are used for parameter identification and validation of the setup dynamics and for analyses of the obtained experimental results.

2.3 Summary

In this section, the design of the experimental setup is discussed. First, a model of the experimental setup, based on the 18-DOF FEM drill-string model, is presented. The 4-DOF setup model is designed such that it represents the dominant dynamics of the dynamics of an oil-field drill-string system that exhibits torsional vibrations. The non-smooth model of the experimental drill-string setup is scaled to feasible dimensions in support of the design of the lab-scale setup. Finally, the mechanical and electrical design of the designed setup is presented in detail.

3 Output-Feedback Controller Design

In this section, a design approach for torsional controllers, aiming to eliminate torsional stick-slip oscillations, is described. In Sect. 3.1, a model reformulation is presented rendering the model suitable in the scope of controller synthesis. Section 3.2

details the control problem formulation in system-theoretic terms. Next, Sect. 3.3 describes the proposed output-feedack control strategy inducing robustness with respect to uncertainties in the bit-rock interaction torque.

3.1 Non-smooth Modelling for Control

The dynamic model of the setup in second -order form, as given in (15)–(17), can be cast into a first-order Lur'e-type system form as follows:

$$\begin{aligned} \dot{x} &= Ax + Gv + G_2 v_2 + Bu_t \\ q &= Hx \\ q_2 &= H_2 x \\ y &= Cx \\ v &\in -\varphi(q) \\ v_2 &\in -\phi(q_2). \end{aligned} \tag{18}$$

Herein, $x = \left[\theta_{s,1} - \theta_{s,2},\ \dot{\theta}_{s,1},\ \dot{\theta}_{s,2},\ \theta_{s,2} - \theta_{s,3},\ \dot{\theta}_{s,3},\ \theta_{s,3} - \theta_{s,4},\ \dot{\theta}_{s,4}\right]^\top \in \mathbb{R}^7$ is the state, where $\theta_{s,i}$, $i = 1, 2, 3, 4$, describes the rotational displacement of the inertias of the setup, and the bit velocity is defined as $q := \dot{\theta}_{s,1}$. Furthermore, $q_2 := \left[\dot{\theta}_{s,2}\ \dot{\theta}_{s,3}\ \dot{\theta}_{s,4}\right]^\top$. Note that only relative angular positions are taken into account, such that the 4-DOF system is described with only 7 state variables. Moreover, the bit-rock interaction torque $\hat{T}_{bit}$ is denoted by $v \in \mathbb{R}$ and the drill-string-borehole interaction torques $\hat{T}_{ws}$ are denoted by $v_2 \in \mathbb{R}^3$. As a consequence, the nonlinearities $\varphi(\cdot)$ and $\phi(\cdot)$ are defined by the set-valued nonlinearities in the right-hand sides of (16) and (17), respectively. In addition, $u_t := \hat{T}_{td} \in \mathbb{R}$ is the (top drive torque) control input and $y := \left[\ \omega_{td}\ T_{pipe}\right]^\top \in \mathbb{R}^2$ is the measured output, where $\omega_{td} := \dot{\theta}_{s,4}$ is the top drive angular velocity. The so-called pipe torque T_{pipe} is the torque in the drill-string directly below the top drive (sometimes also referred to as the saver sub torque). In the experimental setup, this torque is measured using a torque sensor directly below the top-most inertia.

3.2 Control Problem Formulation

The desired operation of the drill-string system is a constant angular velocity ω_{eq} for all four inertias. So, the objective is to regulate this set-point of the non-smooth drill-string system by means of an output-feedback controller. The available output measurements for the controller are the top drive angular velocity ω_{td} and the pipe torque T_{pipe}. The system can be controlled by the top drive torque u_t. The controller should:

1. locally stabilize the desired velocity of the drill-string, therewith eliminating torsional (stick-slip) vibrations;
2. ensure robustness with respect to uncertainty in the non-smooth bit-rock interaction φ;
3. guarantee the satisfaction of closed-loop performance specifications, in particular, on measurement noise sensitivity, i.e., limitation of the amplification of measurement noise, and limitation of the control action such that top drive limitations can be satisfied;
4. guarantee robust stability and performance in the presence of multiple flexibility modes dominating the torsional dynamics.

To facilitate controller synthesis, the drill-string dynamics (18) are reformulated. The desired constant angular velocity ω_{eq} for all discs can be associated with a desired equilibrium x_{eq} for the state of the system. To ensure that x_{eq} is an equilibrium of the closed-loop system, the control input $u_t = u_c + \tilde{u}$ is decomposed in a constant feedforward torque u_c (inducing x_{eq}) and the feedback torque $\tilde{u}$. For the feedforward design, we assume that $\dot{\theta}_{s,i} > 0$, for $i = 2, 3, 4$, hence ϕ is constant and can be compensated for by constant u_c, and we determine x_{eq} and u_c using the equilibrium equation of system (18), i.e., $Ax_{eq} - G\varphi(Hx_{eq}) - G_2\phi(H_2x_{eq}) + Bu_c \ni 0$. Next, we define $\xi := x - x_{eq}$ and apply a linear loop transformation such that the slope of a transformed nonlinearity $\tilde{\varphi}(q)$ (associated with $\varphi(q)$ through the loop transformation) is equal to zero at the equilibrium velocity, i.e., $\partial\tilde{\varphi}/\partial q|_{q=\omega_{eq}} = 0$. This results in a state-space representation of the transformed drill-string dynamics in perturbation coordinates:

$$\dot{\xi} = A_t\xi + B\tilde{u} + G\tilde{v} \tag{19a}$$
$$\tilde{y} = C\xi \tag{19b}$$
$$\tilde{q} = H\xi \tag{19c}$$
$$\tilde{v} \in -\tilde{\varphi}\left(\tilde{q}\right) \tag{19d}$$

with $A_t := A + \delta GH$, $\delta = -\partial\varphi/\partial q|_{q=\omega_{eq}} > 0$, $\tilde{y} := y - Cx_{eq}$, $\tilde{q} := q - Hx_{eq}$, $\tilde{\varphi}\left(\tilde{q}\right) := \varphi\left(\tilde{q} + Hx_{eq}\right) - \varphi\left(Hx_{eq}\right) + \delta\tilde{q}$ and $\tilde{v} := v - v_{eq} - \delta\tilde{q}$. The dynamics in (19) represents a Lur'e-type system, with the linear dynamics (19a)–(19c), with transfer function G_{ol}, and having inputs $\tilde{u}$ and $\tilde{v}$ and outputs $\tilde{y}$ and $\tilde{q}$, and the nonlinearity $\tilde{\varphi}$ in the feedback loop. The open-loop transfer function $G_{ol}(s)$ is defined as

$$\begin{bmatrix} \tilde{q}(s) \\ \tilde{y}(s) \end{bmatrix} := G_{ol}(s) \begin{bmatrix} \tilde{v}(s) \\ \tilde{u}(s) \end{bmatrix} = \begin{bmatrix} g_{11}(s) & g_{12}(s) \\ g_{21}(s) & g_{22}(s) \end{bmatrix} \begin{bmatrix} \tilde{v}(s) \\ \tilde{u}(s) \end{bmatrix}. \tag{20}$$

In the context of the second controller objective above, we model the nonlinearity $\tilde{\varphi}$ (Fig. 16a) by an uncertainty Δ (Fig. 16b). This model formulation is used in the controller design approach developed in Sect. 3.3. Note that $\tilde{\varphi}$ describes a nonlinear (set-valued) mapping from $\tilde{q}$ to $\tilde{v}$, while the uncertainty Δ is assumed to be a (complex) LTI uncertainty (with output $\check{v}$). This means that, for example, stability of

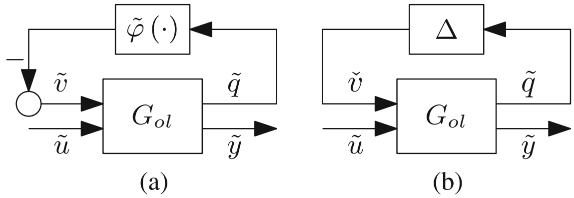

Fig. 16 Block diagram of the system dynamics (19) in Lur'e type form (**a**) and the linear dynamics G_{ol} with (complex) model uncertainty Δ (**b**)

the closed-loop system with uncertainty Δ does not directly imply stability for the closed-loop system with nonlinearity $\tilde{\varphi}$. Nevertheless, the model in Fig. 16b is used as a basis for controller synthesis in the next section. Subsequently, the stability of the nonlinear (non-smooth) closed-loop system is analyzed in detail in Sect. 3.3.3.

3.3 Design of a Robust Output-Feedback Controller

In this section, we present a robust control design approach based on skewed-μ DK-iteration ([38]).

First, we formulate the general control configuration that is used in such a robust control context. Next, in Sect. 3.3.1, we analyze nominal performance of the (linear) system, i.e., without uncertainty. This is extended to robust performance for the (linear) system with uncertainty taken into account in Sect. 3.3.2. The stability of the closed-loop nonlinear system is investigated in Sect. 3.3.3.

This robust control technique combines several concepts from robust control theory to design a controller that achieves robust stability and performance of a system with model uncertainties [34].

Robust control methods focus on the design of controllers, while system uncertainties are explicitly taken into account in the design. The general control configuration for a (LTI) plant P with an uncertainty Δ and (LTI) controller K is shown in Fig. 17, where e is the error in the measured output, u the control output and w and z represent the (weighted) exogenous inputs and outputs. This structure is similar to the block diagram in Fig. 16b with $\bar{v}$ and $\bar{q}$ as weighted representations of $\check{v}$ and $\tilde{q}$ (see Sect. 3.3.2) and, in addition, includes the controller K. The system P, in Fig. 17, is described by

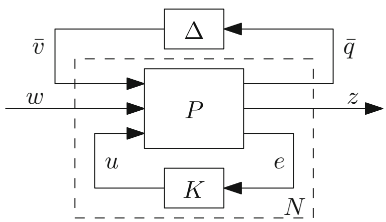

Fig. 17 General control configuration with uncertainty block Δ

$$\begin{bmatrix} \bar{q} \\ z \\ e \end{bmatrix} = \begin{bmatrix} P_{11} & P_{12} & P_{13} \\ P_{21} & P_{22} & P_{23} \\ P_{31} & P_{32} & P_{33} \end{bmatrix} \begin{bmatrix} \bar{v} \\ w \\ u \end{bmatrix}. \tag{21}$$

The system $N := F_l(P, K)$ is defined as the lower linear fractional transformation (LFT) of the plant P with the controller K, that is:

$$N = \begin{bmatrix} P_{11} & P_{12} \\ P_{21} & P_{22} \end{bmatrix} + \begin{bmatrix} P_{13} \\ P_{23} \end{bmatrix} K (I - P_{33}K)^{-1} \begin{bmatrix} P_{31} & P_{32} \end{bmatrix}.$$

With the introduction of the controller K, we can also introduce the closed-loop bit-mobility function. The closed-loop bit-mobility transfer function G_{cl} from the input $\tilde{v}$ to the output $\tilde{q}$, of system (19) with controller K, is defined by

$$G_{cl} := g_{11} - g_{12}K(I + g_{22}K)^{-1}g_{21}. \tag{22}$$

This bit-mobility plays an important role in the stability of the closed-loop system (see Sect. 3.3.3 for the role of G_{cl} in the scope of a nonlinear stability analysis), and is therefore important in the controller design methodology.

3.3.1 Nominal Stability and Nominal Performance

As mentioned above, the controller design aims at stability, performance, and robustness for the uncertainty Δ. In this section, the focus is on the first two aspects. Robustness is considered in the next section. Based on the system representation in Fig. 16b, the closed-loop system of the linear drill-string dynamics G_{ol} in feedback with the linear, dynamic controller K to be designed is shown in Fig. 18. In this representation, additional inputs n and d are introduced, representing measurement noise and actuator noise, respectively.

Consider the system without uncertainty given by

$$\begin{bmatrix} z \\ e \end{bmatrix} := \underline{P} \begin{bmatrix} w \\ u \end{bmatrix} = \begin{bmatrix} P_{22} & P_{23} \\ P_{32} & P_{33} \end{bmatrix} \begin{bmatrix} w \\ u \end{bmatrix} \tag{23}$$

with w and z weighted versions of $\underline{w} := \begin{bmatrix} n & d \end{bmatrix}^\top$ and $\underline{z} := \begin{bmatrix} e & u \end{bmatrix}^\top$, respectively. The weighted inputs and outputs are discussed in more detail in Sect. 3.3.2. Moreover,

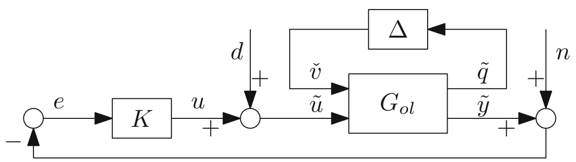

Fig. 18 Linear drill-string dynamics G_{ol} in closed loop with the controller K and including model uncertainty Δ with disturbances d and n

define the lower LFT of $\underline{P}$ with the controller K, that is, $N_{22} := F_l\left(\underline{P}, K\right)$. Next, the concept of nominal performance is defined as follows: for a system without uncertainty Δ, the closed-loop system $N_{22} = F_l(\underline{P}, K)$ is internally stable and the $\mathscr{H}_\infty$-norm of this system (from w to z) is smaller than 1, that is,

$$\|N_{22}\|_\infty = \sup_\omega \bar{\sigma}\left(F_l(\underline{P}, K)\right) < 1, \tag{24}$$

where we used the definition of the $\mathscr{H}_\infty$-norm $\|H(s)\|_\infty := \operatorname{ess\,sup}_{\omega\in\mathbb{R}} \bar{\sigma}\left(H\left(j\omega\right)\right)$ and $\bar{\sigma}$ indicates the maximum singular value. This means that nominal performance can be achieved by solving the "standard" $\mathscr{H}_\infty$ optimal control problem, in which the aim is to find the internally stabilizing controller K that minimizes $\|F_l(\underline{P}, K)\|_\infty$ (see [34] for details). Internal stability of the closed-loop can be guaranteed by a proper choice of the inputs w and outputs z. As proved in [41, Sect. 5.3], by choosing w and z as defined earlier, the $\mathscr{H}_\infty$ controller synthesis guarantees internal stability of the closed-loop system. Specification of the weighting filters is treated in more detail in Sect. 3.3.2. Moreover, the system *with* uncertainty is addressed in the next section, leading to the concept of (alternative) robust performance.

3.3.2 Alternative Robust Performance

Robust performance means that the stability and performance objective, addressed in Sect. 3.3.1, is achieved for all possible models in the uncertainty set $\mathbf{D}$ [34], i.e., for all $\Delta \in \mathbf{D}$. Standard robust performance techniques typically aim at optimizing the performance for all possible plants induced by the uncertainty set. In contrast, we aim to optimize the robustness with respect to the uncertainty while still guaranteeing internal stability and satisfaction of given performance objectives. This is what we call *alternative robust performance*. In the drilling context, this means that, for example, a (fixed) bound on the control action should be satisfied (see controller objective 3 in Sect. 3.2), while the robustness with respect to the nonlinear bit-rock interaction is optimized (as specified in the second controller objective).

Consider the system P in Fig. 17, including the uncertainty block, Δ. The input-output pair $\bar{v}$, $\bar{q}$ is related to this uncertainty block and the (weighted) closed-loop transfer function $N(s) = F_l\left(P, K\right)$ is given by

$$\begin{bmatrix} \bar{q} \\ w \end{bmatrix} = N \begin{bmatrix} \bar{v} \\ z \end{bmatrix} = F_l\left(P, K\right) \begin{bmatrix} \bar{v} \\ z \end{bmatrix}. \tag{25}$$

Robust stability is obtained by designing a controller K such that the system N is internally stable and the upper LFT, $F := F_u(N, \Delta)$, is stable for all $\Delta \in \mathbf{D}$. Herein, the uncertainty set $\mathbf{D}$ is a norm-bounded subset of $\mathscr{H}_\infty$,[1] i.e., $\mathbf{D} =$

[1] $\mathscr{H}_\infty$ is a (closed) Banach space of matrix-valued functions that are analytic in the open right-half plane and bounded on the imaginary axis. The real rational subspace of $\mathscr{H}_\infty$ is denoted by $\mathscr{RH}_\infty$, which consists of all proper and real rational stable transfer matrices [41, Sect. 4.3].

$\{\Delta \in \mathscr{RH}_\infty | \|\Delta\|_\infty < 1\}$. The aim is to find a stabilizing controller that also meets certain performance specifications. Therefore, we use a similar approach as in [34, Sect. 8.10] and consider the fictitious 'uncertainty' Δ_P. The uncertainty Δ_P is a complex unstructured uncertainty block which represents the $\mathscr{H}_\infty$ performance specifications. Moreover, note that $\Delta_P \in \mathbf{D}_P$, with $\mathbf{D}_P = \{\Delta_P \in \mathscr{RH}_\infty \,|\|\Delta_P\|_\infty \leq 1\}$. The result given in [41, Theorem 11.8] states that a robust performance problem is equivalent to a robust stability problem with the augmented uncertainty

$$\hat{\Delta} = \begin{bmatrix} \Delta & 0 & 0 \\ 0 & & \\ 0 & \multicolumn{2}{c}{\Delta_P} \end{bmatrix} \tag{26}$$

with $\hat{\Delta}$ a block-diagonal matrix. In other words, both the performance specifications and uncertainty are taken into account in a similar fashion. Moreover, $\hat{\mathbf{D}}$ is the uncertainty set with a structure as given in (26) and any $\Delta \in \mathbf{D}$ and $\Delta_P \in \mathbf{D}_P$. The robust performance condition can now be formulated as follows:

$$\mu_{\hat{\mathbf{D}}}\left(N(j\omega)\right) \leq 1, \quad \forall\omega, \tag{27}$$

where $\mu_{\hat{\mathbf{D}}}$ is the structured singular value with respect to $\hat{\mathbf{D}}$. The structured singular value is defined as the real non-negative function

$$\mu_{\hat{\mathbf{D}}}(N) = \frac{1}{\bar{k}_m},\ \bar{k}_m = \min\left\{k_m \,\middle|\det\left(I - k_m N\hat{\Delta}\right) = 0\right\} \tag{28}$$

with complex matrix N and block-diagonal uncertainty $\hat{\Delta}$.

To optimize the robustness with respect to the uncertainty Δ (i.e., part of $\hat{\Delta}$ in (26)), the skewed structured singular value μ^s can be used. The skewed structured singular value is used if some uncertainty blocks in $\hat{\Delta}$ are kept fixed (Δ_P in this case) to investigate how large another source of uncertainty (Δ in this case) can be, before robust stability/performance can no longer be guaranteed. In this case, we aim to optimize the robustness of the closed-loop system with respect to uncertainty Δ in the bit-rock interaction. Thus, we aim to obtain the largest uncertainty set Δ, given a fixed Δ_P (i.e., fixed performance specifications). Therefore, we introduce the matrix $K_m^s := \text{diag}\left(k_m^s,\ I\right)$, and the skewed structured singular value $\mu^s_{\hat{\Delta}}(N)$ is defined as

$$\mu^s_{\hat{\mathbf{D}}}(N) = \frac{1}{\bar{k}^s_m},\ \bar{k}^s_m = \min\left\{k^s_m \,\middle|\det\left(I - K^s_m N\hat{\Delta}\right) = 0\right\}. \tag{29}$$

Thus, the robust performance condition (27), with additional scaling (through K_m^s) in terms of the skewed structured singular value, is written as the *alternative* robust performance condition

$$\mu^s_{\hat{\mathbf{D}}}\left(N(j\omega)\right) \leq 1, \quad \forall\omega. \tag{30}$$

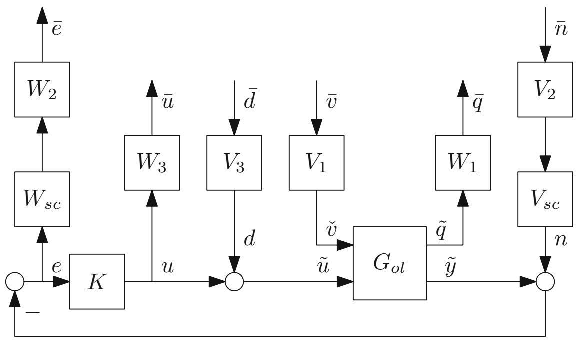

Fig. 19 Closed-loop system with weighting filters and scaling matrices

To support controller design satisfying particular performance specifications, weighting filters and scaling matrices are introduced in the loop in Fig. 18, as shown in Fig. 19. Those frequency-domain weighting filters allow us to specify the (inverse) maximum allowed magnitudes of the closed-loop transfer functions. Moreover, the scaling matrices are introduced to improve the numerical conditioning of the problem and to tune the desired bandwidth. The (weighted) generalized plant P with input weighting filters $V_i(s)$ and output weighting filters $W_i(s)$, with $i \in \{1, 2, 3\}$, and scaling matrices W_{sc} and V_{sc}, is specified by

$$\begin{bmatrix} \bar{q} \\ \bar{e} \\ \bar{u} \\ e \end{bmatrix} = \underbrace{\begin{bmatrix} W_1 & 0 & 0 & 0 \\ 0 & W_2 W_{sc} & 0 & 0 \\ 0 & 0 & W_3 & 0 \\ 0 & 0 & 0 & I_2 \end{bmatrix} \bar{P} \begin{bmatrix} V_1 & 0 & 0 & 0 \\ 0 & V_{sc} V_2 & 0 & 0 \\ 0 & 0 & V_3 & 0 \\ 0 & 0 & 0 & 1 \end{bmatrix}}_{P} \begin{bmatrix} \bar{v} \\ \bar{n} \\ \bar{d} \\ u \end{bmatrix}.$$

Herein, $\bar{P}(s)$ is the MIMO transfer function of the unweighted system $\bar{P}$ with inputs $\begin{bmatrix} \tilde{v} & n & d & u \end{bmatrix}^\top$ and outputs $\begin{bmatrix} \tilde{q} & e & u & e \end{bmatrix}^\top$ with its state-space realization given by

$$\bar{P} \overset{s}{=} \left[\begin{array}{c|cccc} A_t & G & 0 & B & B \\ \hline H & 0 & 0 & 0 & 0 \\ -C & 0 & -I & 0 & 0 \\ 0 & 0 & 0 & 0 & I \\ -C & 0 & -I & 0 & 0 \end{array} \right]. \tag{31}$$

In this section, we have introduced an alternative robust performance framework. To design a controller that minimizes the skewed structured singular value $\mu^s_{\hat{\mathbf{D}}}$, for the purpose of obtaining robust performance, a procedure for synthesizing such a controller, known as the DK-iteration procedure [34, Sect. 8.12], is treated concisely below.

The first step in such a DK-iteration procedure is the introduction of D-scaling matrices. This scaling uses the fact that $\hat{\Delta}$ is structured, hence, the inputs and out-

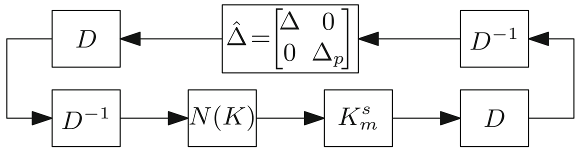

Fig. 20 Block diagram of the implementation for the skewed-μ DK-iteration procedure

puts to $\hat{\Delta}$ and N are scaled by inserting the matrices D and D^{-1}, as shown in Fig. 20. Using such scaling generally enables one to find potentially tighter robust stability/performance conditions. For further details on the procedure, the reader is referred to [24, 34].

The skewed-μ DK-iteration procedure aims at designing a controller that minimizes the peak value over frequency of the upper bound on the skewed structured singular value, i.e., a controller K should be designed by solving the following optimization problem:

$$\min_K \left(\min_D \|DK_m^s N(K) D^{-1}\|_\infty \right). \tag{32}$$

Here, the original scaling matrix $D(\omega)$ is replaced by a stable minimum-phase transfer function fit $D(s)$ of $D(\omega)$. The dependency of the closed-loop transfer function N on the controller K is indicated by $N(K)$. In DK-iterations, a μ-analysis (D-step) and $\mathscr{H}_\infty$-optimization (K-step) are solved alternately (see [24]). In other words, the skewed-μ DK-iteration procedure alternates between minimizing (32) with respect to either K or D (while holding the other fixed) and recursively updating k_m^s (which characterizes K_m^s) during the D-step.

3.3.3 Closed-Loop Stability Analysis

The main purpose of the controller is to stabilize the equilibrium $\xi = 0$ of the nonlinear system (19). Let us that assume that a controller K has been designed that meets the performance specifications and is robust with respect to the uncertainty Δ. Hence, the designed controller guarantees stability for the *linear* closed-loop system $N(s)$ and achieves robustness with respect to the uncertainty Δ. In this section, the stability of the *nonlinear* closed-loop system is considered. Therefore, we define a symmetric sector condition on the nonlinearity $\tilde{\varphi}$ such that, for any (locally Lipschitz) nonlinearity which (locally) satisfies this sector condition, (local) asymptotic stability of the origin of the closed-loop system can be guaranteed.

We use the circle criterion [16, Theorem 7.1] to determine a (symmetric) sector on the nonlinearity $\tilde{\varphi}$ for which robust stability can be guaranteed. Consider the closed-loop bit-mobility (22) and a symmetric sector condition on the nonlinearity which is satisfied for all $\tilde{q} \in \mathscr{S}$ with $\mathscr{S} := \{\tilde{q} \in \mathbb{R} | \tilde{q}_l < \tilde{q} < \tilde{q}_u\}$ and $\tilde{q}_l < 0 < \tilde{q}_u$, i.e. $\tilde{\varphi}(\tilde{q}) \in [-\gamma, \gamma]$ $\forall\, \tilde{q} \in \mathscr{S}$ and $\gamma > 0$. We note that, although $\tilde{\varphi}$ is a set-valued nonlinearity, we have that, for $\omega_{eq} > 0$ (i.e., for a nominal velocity away from the discontuinity in the bit-rock interaction at zero velocity), there indeed exist $\tilde{q}_l$ and $\tilde{q}_u$ such that the latter symmetric sector condition is satisfied. The nonlinear system is locally absolutely stable (i.e., $\xi = 0$ is locally asymptotically stable for any $\tilde{\varphi}(\tilde{q}) \in [-\gamma, \gamma]$ with $\tilde{q} \in \mathscr{S}$) if

$$H(s) = (1 + \gamma G_{cl}(s))\,(1 - \gamma G_{cl}(s))^{-1}, \tag{33}$$

is strictly positive real. Applying Lemma 6.1 in [16], a scalar transfer function $H(s)$ is strictly positive real if the following conditions are satisfied:

1. $H(s)$ is Hurwitz;
2. $\mathrm{Re}\,[H(j\omega)] = \mathrm{Re}\left[\frac{1+\gamma G_{cl}(j\omega)}{1-\gamma G_{cl}(j\omega)}\right] > 0, \quad \forall \omega \in \mathbb{R}$;
3. $H(\infty) > 0$.

For the symmetric sector, the condition on $H(s)$ being Hurwitz is equivalent to $G_{cl}(s)$ being Hurwitz. The closed-loop transfer function $G_{cl}(s)$ of the feedback interconnection is Hurwitz by the design of the stabilizing controller K. Moreover, G_{cl} is strictly proper, and therefore $H(\infty) = 1$, such that the third condition is satisfied. The second condition is equivalent to the condition:

$$\|G_{cl}(j\omega)\|_\infty < \frac{1}{\gamma}. \tag{34}$$

Hence, the $\mathscr{H}_\infty$-norm of the closed-loop bit-mobility G_{cl} gives an upper bound on the sector that the nonlinearity $\tilde{\varphi}$ should comply with, for the system to be absolutely stable. With the DK-iteration procedure, presented above, a controller K can be designed such that $\|G_{cl}\|_\infty$ is indeed minimized. In other words, the robustness with respect to uncertainty in the bit-rock interaction is optimized. This shows the benefit of employing the alternative robust performance technique (see Sect. 3.3.2) in terms of optimizing the robustness of the closed-loop drill-string dynamics with respect to the uncertainty in the bit-rock interaction, also in the nonlinear context.

In the following section, design guidelines for the tuning of the weighting filters tailored to the drilling context are given, and the designed controller is presented and validated through experiments.

4 Experimental Controller Validation

In this section, the implementation and experimental results obtained with the controller design strategy of the previous section are presented. First, a startup scenario for the experiments on the drill-string setup is discussed in Sect. 4.1. Next, in Sect. 4.2, the implementation of the SoftTorque controller, being the industrial standard, is discussed, and an experimental result of this industrial controller having been applied to the setup is shown. Finally, in Sect. 4.3, the implementation and experimental results are discussed for the linear robust output-feedback controller, as presented in Sect. 3.

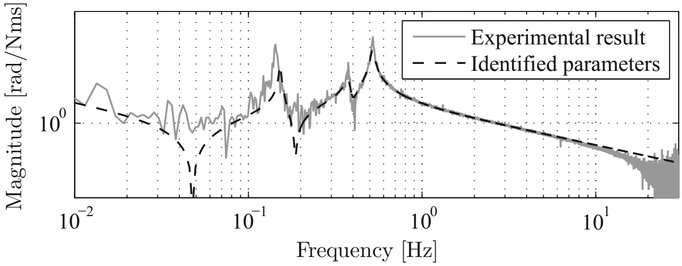

Fig. 21 Open-loop bit-mobility of the setup, i.e., the frequency response function from bit torque T_{bit} to bit velocity ω_{bit}

Before going into detail about the implementation of the controllers and the experimental results, let us consider the (open-loop) bit-mobility of the experimental drill-string setup. As advocated earlier, the bit-mobility plays an important role in the onset of stick-slip vibrations and the proposed control strategy aims to minimize its $\mathcal{H}_\infty$-norm. The measured open-loop bit-mobility of the setup is shown in Fig. 21. In the same figure, the bit-mobility of the setup model based on experimentally identified parameters is shown. For details on the performed parametric model identification, we refer to [37]. Clearly, the third resonance mode is well captured by the model and the second flexibility mode is more damped in the model compared to the actual bit-mobility of the setup. Moreover, the first resonance mode exhibits some discrepancy between the model and the experiments. Here, we opt for an identified model that aims to capture, in particular, the third resonance mode accurately, as it is precisely this dominant mode (in the bit-mobility) that is responsible for the occurrence of stick-slip oscillations. Moreover, it is well-known that it is relatively easy to design a controller that robustly damps the first mode despite such uncertainties (already guaranteed by a Soft-Torque controller).

4.1 Experimental Startup Scenario Description

For the experiments, we introduce a so-called startup scenario, which is based on practical startup procedures for drilling rigs. Herein, the drill-string is first accelerated to a low constant rotational velocity with the bit above the formation (off bottom) and, subsequently, the angular velocity and weight-on-bit (WOB) are gradually increased to the desired operating conditions. The increase in WOB is modelled as a scaling of the bit-rock interaction torque (TOB).

The startup scenario for the experiments is visualized in Fig. 22. The reference angular velocity of the upper discs is shown in the upper plot and the scaling of the TOB, indicated by α, is shown in the bottom plot. The timing of the transitions in the startup scenario can be summarized as follows:

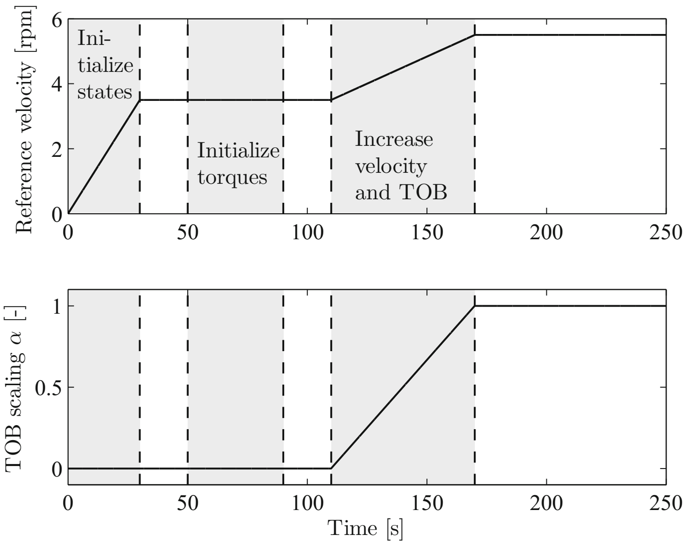

Fig. 22 Reference velocity and TOB scaling of the startup scenario for the experimental setup

1. Start with zero initial velocities and linearly increase the reference angular velocity from zero to 3.5 rpm[2] in the period between $t = 0$ and $t = 30$ s. At the same time, increase the feedforward torque (u_c) to its nominal value;
2. Between $t = 50$ and $t = 90$ s, adapt the drill-string borehole interaction torques T_w to obtain the desired values, based on the torque sensor readings, in order to compensate for possibly changed friction characteristics (in the bearings supporting the discs);
3. Gradually increase the reference angular velocity until the desired operating velocity (ω_{eq} being 5.5 rpm) is reached (in the time window $110 \leq t < 170$ s). At the same time, gradually change the TOB to emulate that the bit bites the formation, and finally, obtain the nominal operating condition in both the angular velocity and the TOB. Adapting the torque on bit is done as follows. The bit-rock interaction model is scaled by using the scaling factor $\alpha(t)$ according to:

$$\hat{T}_{bit}(t) = \text{Sign}(\omega_{bit}) \left(T_{ini} + \alpha(t) \left(\hat{T}_d - T_{ini} + \left(\hat{T}_s - \hat{T}_d \right) e^{-\frac{30}{\hat{N}_d \pi} |\omega_{bit}|} \right) \right), \quad (35)$$

where T_{ini} is the amount of resisting torque that is still present at the bit-rock interface, even when the bit is off bottom (e.g., due to drilling mud and interactions with the borehole). For WOB $= 0$ (off bottom; characterized by $\alpha = 0$), there is no velocity-weakening in the TOB. The scaling factor $\alpha(t)$ in (35) is given by

[2] Note that due to scaling, this corresponds to 35 rpm on a real drilling rig.

$$\alpha(t) = \begin{cases} 0, & t_0 \le t \le t_1 \\ \frac{t-t_1}{t_2-t_1}, & t_1 < t < t_2 \\ 1, & t \ge t_2 \end{cases} \tag{36}$$

with $t_1 = 110$ and $t_2 = 170$ in this case.

4.2 SoftTorque Controller

The SoftTorque controller ([14]) is a controller for drill-string systems, widely used in industry. This controller aims at damping of the first torsional flexibility mode of the drill-string system only. This active damping system is a PI-controller, based only on the velocity error e_y between the measured top drive velocity $y = \omega_{td}$ and the reference angular velocity $\omega_{td,ref}$, i.e., $e_y := \omega_{td,ref} - \omega_{td}$. The controller is given by the transfer function

$$T_{fb}(s) = \left(c_t + \frac{k_t}{s}\right) e_y(s), \ s \in \mathbb{C}, \tag{37}$$

with $c_t = 2.93$ and $k_t = 1.87$ tuned such that damping of the first torsional flexibility mode of the setup is obtained (note that these controller parameter settings corresponds to unscaled system parameters, as mentioned in Sect. 2.1.4). In Fig. 23, the measured closed-loop bit-mobility of the drill-string setup with the SoftTorque controller is shown. It is clearly visible that the first torsional mode is damped using the SoftTorque controller, but the amplitude of the second and third modes are similar in the open-loop and closed-loop cases, illustrating a key deficiency of the SoftTorque controller.

An experimental result of the closed-loop drill-string system with SoftTorque controller (with the same constant feedforward active as for the controller proposed in Sect. 3) is shown in Fig. 24. In the response of the bit angular velocity, stick-slip oscillations can be observed. The onset of these oscillations starts when the reference

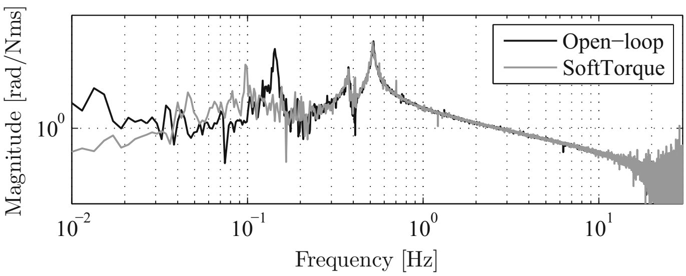

Fig. 23 Bit-mobility of the setup with SoftTorque controller

angular velocity and scaling factor α (for emulating an increase of the WOB) start to increase at $t = 110$ s. This experimentally shows that the SoftTorque controller is indeed unable to avoid stick-slip oscillations for the setup.

In Fig. 24, the filtered and unfiltered responses of the system are shown. The filtered response of the system is compared with a simulation result of the model of the setup with the identified parameters. The results are shown side-by-side in Fig. 25. To allow for a clear comparison, a shift of the time axis has been applied for

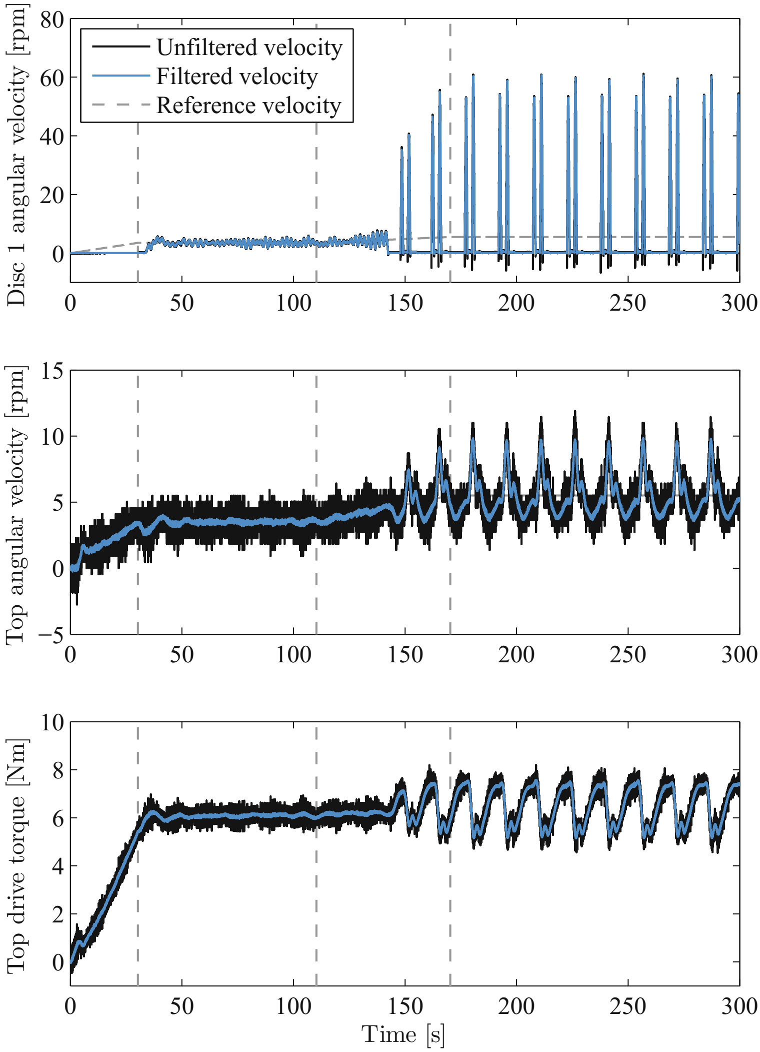

Fig. 24 Experimental result of the drill-string setup with the SoftTorque controller in the startup scenario

the experimental results. As can be seen from this figure, the closed-loop response of the experimental setup is very similar to the response of the simulation results. The only difference is the somewhat shorter sticking period in the simulation results between two successive groups of two slipping periods (i.e., the long sticking period). This result further illustrates that the setup is capable of accurately emulating the non-smooth drill-string dynamics to be investigated, also in closed-loop operation.

4.3 $\mathscr{H}_\infty$-Based Output-Feedback Controller

The linear robust output-feedback controller design methodology, presented in Sect. 3.3, is also used to design a controller for the experimental drill-string setup. The results of the drill-string setup in closed loop with the $\mathscr{H}_\infty$-based controller are presented in this section.

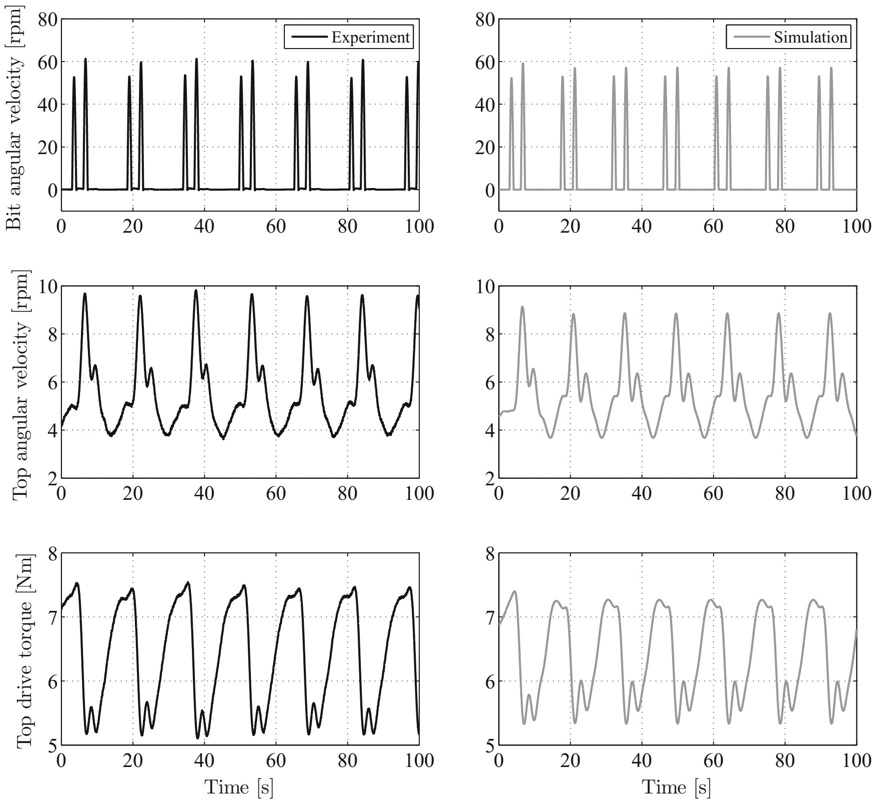

Fig. 25 Comparison between the experimental result and simulation result of the drill-string model with the SoftTorque controller

Weighting filter design is key to satisfying the performance specifications related to, e.g., measurement noise sensitivity and actuator limitations. Moreover, achieving specific design targets such as the inclusion of integral action and high-frequency roll-off can be achieved by absorbing these filters into the loop see [21]. High-frequency roll-off reduces measurement noise amplification. Also, integral action is desired from a practical point of view, e.g., in case of a mismatch between the (model-based) feedforward torque u_c and the actual required feedforward torque due to uncertainty in the respective models for the bit-rock interaction and the drill-string borehole interaction. In that case, integral action will compensate for this mismatch so as to obtain convergence to the desired setpoint.

For the design of a controller for the drill-string model (18), the following objectives are set:

- Integral action for low-frequencies;
- Second-order roll-off for high freqencies
- Cross-over frequency of the open-loop transfer function KG_{ol} (at the plant input) at 0.6 Hz, i.e., just above the third eigenfrequency of the drill-string system (see Fig. 11);
- Plant output scaling, i.e., scale the plant output $y = \begin{bmatrix}\omega_{td} \; T_{pipe}\end{bmatrix}^\top$ such that the components of the weighted plant output are of the same order of magnitude.

These objectives are obtained through specific choices for several settings of the weighting filters, as displayed in Fig. 19.

First, we apply plant scaling by using the scaling matrices W_{sc} and V_{sc}. This scaling is applied to compensate for the different order of magnitude of the two plant outputs ω_{td} and T_{pipe}. This is important for a system with multiple outputs in a norm-based controller synthesis method such as skewed-μ DK-iteration. When the plant outputs are not scaled and the outputs differ in order of magnitude, one off-diagonal term in the closed-loop sensitivity function will be large and the other small. In the synthesis, it is then possible that the emphasis is on reducing the large off-diagonal element at the expense of other elements. The plant scaling matrices W_{sc} and V_{sc} are tuned to compensate for this effect. The matrices are given by

$$W_{sc} = \begin{bmatrix} w_{sc1} & 0 \\ 0 & w_{sc2} \end{bmatrix}, \quad V_{sc} = \begin{bmatrix} 1 & 0 \\ 0 & 1 \end{bmatrix}.$$

The filters $V_i(s)$ and $W_i(s)$, $i = 1, 2, 3$, are so-called performance filters and are used to tune the performance-related properties of the closed-loop system. The filters $V_1(s)$ and $W_1(s)$ can be used to tune the closed-loop bit-mobility (G_{cl}). Ideally, the bit-mobility should be damped as much as possible (as follows from the stability analysis in Sect. 3.3.3). However, this typically results in high control action. To deal with this trade-off, the weighting filter $V_1(s)$ has a notch filter and is defined as follows:

$$\begin{aligned} V_1 &= v_1 V_{notch} \\ &= v_1 \frac{\frac{1}{(2\pi f_1)^2}s^2 + \frac{2b_1}{2\pi f_1}s + 1}{\frac{1}{(2\pi f_2)^2}s^2 + \frac{2b_2}{2\pi f_2}s + 1}, \end{aligned} \tag{38}$$

where f_j ($j = 1, 2$) is the frequencies of the notch filter $V_{notch}(s)$ and b_1 and b_2 the parameters for tuning the depth of the notch filter. The output weighting filter $W_1(s)$ is set to a constant w_1.

The remaining weighting filters are the filters for tuning the closed-loop performance transfer functions. Let us first focus on the input weighting filters $V_2(s)$ and $V_3(s)$. The filter $V_2(s)$ is given by

$$V_2 = \begin{bmatrix} v_{21} & 0 \\ 0 & v_{22} \end{bmatrix}, \tag{39}$$

where v_{21} and v_{22} are static gains. These gains, as well as static gains in other weighting filters, are used to scale those filters. Scaling is necessary to obtain a feasible controller design with respect to the performance uncertainty $\Delta_P(s)$ and changing the gains allows for the synthesis of different controllers. The input weighting filter $V_3(s)$ is set as

$$V_3(s) = v_3 \|g_{co}\|^{-1} \frac{1}{w_{sc1}}, \tag{40}$$

where v_3 is a static gain and $g_{co} := g_{22,1}(j2\pi f_{co})$, i.e., the sub plant gain, related to input $\tilde{u}$ and output $\tilde{y}_1 = \omega_{td} - \omega_{eq}$, at the target cross-over frequency f_{co}. This gain is chosen to obtain a cross-over frequency of the open-loop transfer function KG_{ol} at 0.6 Hz, as specified. This cross-over frequency is chosen to achieve damping of the dominant resonance modes.

The output weighting filters $W_2(s)$ and $W_3(s)$ are also used to tune the closed-loop transfer functions, as well as to meet the first two controller objectives, i.e., to include integral action and first-order roll-off. The controller $K_t(s)$ to be designed has two inputs and a single output (due to the two measured signals of the plant), i.e., $K_t(s) = \left[K_{\omega_{td}}(s)\ K_{T_{pipe}}(s)\right]$. The controller aims at stabilizing the desired angular velocity setpoint. Hence, an integrator should be specified in the top drive angular velocity control loop. Note that it is not possible (and not necessary) to include an integrator in both control loops $K_{\omega_{td}}(s)$ and $K_{T_{pipe}}(s)$. An integrator would force the sensitivity function to zero for $s = 0$; however, this is not possible for both sensitivity functions, due to the fact that we are dealing with a non-square plant. In other words, there is only one control signal that can eliminate the steady-state error for one of the two measurements. However, forcing ω_{td} to its equilibrium value also results in T_{pipe} converging to its equilibrium. So, by only requiring integral action in the control loop related to ω_{td}, the output weighting filter $W_2(s)$ is given by

$$W_2(s) = \begin{bmatrix} W_I(s) & 0 \\ 0 & w_{22} \end{bmatrix} = \begin{bmatrix} P_I \frac{s+2\pi f_I}{s} & 0 \\ 0 & w_{22} \end{bmatrix}, \tag{41}$$

using $W_I(s)$ to obtain an integral action in $K_{\omega_{td}}(s)$ and w_{22} a static gain. To obtain high-frequency roll-off, a roll-off filter is included in the output filter $W_3(s)$, hence

$$W_3(s) = w_3 w_{sc1} \|g_{co}\| W_R^{-1}, \tag{42}$$

where w_3 is a static gain, and $W_R = \frac{(2\pi f_R)^2}{s^2+4\pi\beta f_R s+(2\pi f_R)^2}$ the second-order roll-off filter with roll-off frequency f_R.

The weighting filters $W_2(s)$ and $W_3(s)$ are unstable and non-proper weighting filters, respectively. Therefore, these filters are not applicable in the $\mathscr{H}_\infty$-controller synthesis. To circumvent this limitation and still obtain a controller that includes integral action and high-frequency roll-off, we add filters in the loop [21]. We require high-frequency roll-off on both input signals (top drive velocity and pipe torque) of the controller and integral action on the top drive velocity. To acheive this, the actual plant that is used in the controller synthesis algorithm is given by

$$G_t(s) = \text{diag}\left(1,\ W_I(s),\ 1\right) G_{ol}(s)\text{diag}\left(1, W_R(s)\right), \tag{43}$$

where $W_R(s)$ and $W_I(s)$ are the roll-off and integrator filters, respectively. The resulting controller $K(s)$ from the DK-iteration procedure, treated in Sect. 3.3.2, for this plant G_t, has no integrator and roll-off properties. However, the actual controller (for the plant G_{ol}) can be calculated as follows:

$$K_t(s) = W_R(s)K(s)\text{diag}\left(W_I(s),\ 1\right), \tag{44}$$

which does include the desirable integrator and roll-off properties.

Now, two different controllers will be synthesized based on the skewed-μ DK-iteration procedure and the proposed weighting filters from the previous section. Of course, it is possible to change all weighting filters so as to obtain a different controller; however, the weighting filters have been chosen such that the controller objectives can be met, and tuning of the parameters already allows us to synthesize different controllers. The two controllers mainly differ in the allowed control action and will be referred to as a *high-gain* (hg) controller and a *low-gain* (lg) controller. The extra allowed control action for the high-gain controller is used for even greater suppression of the bit-mobility compared to the low-gain controller. In Table 3, the parameters of the weighting filters are given for both controllers. The notch filter in $V_1(s)$ is used to allow for a higher bit-mobility within specific frequency ranges.

Performing the DK-iteration procedure for the drill-string system with the weighting filters as specified above, results in the controller $K_t(s) = \left[K_{\omega_{td}}(s),\ \ K_{T_{pipe}}(s)\right]$, as shown in Fig. 26 for both the high-gain and the low-gain controller. These controllers only use the measured top drive angular velocity ω_{td} and the pipe torque measurement T_{pipe}. In the experimental setup, the pipe torque measurement is based on the torque sensor reading just below the upper disc, compensated for the additional damping term between disc 1 and 4. From this figure, the integral action in the controller, $K_{\omega_{td}}(s)$, which uses the top drive angular velocity, can be clearly recognized. This feature is also present (single-input-single-output) in the SoftTorque controller, also depicted in Fig. 26. This figure shows that both the high-gain and the low-gain controller have a second-order roll-off filter. It can also be observed that the designed

Table 3 Parameter settings for the performance weighting filters for the designed high-gain and low-gain controller

Filter/setting	Parameters	
	Low-gain controller	High-gain controller
W_{sc}	$w_{sc1} = 1, w_{sc2} = 10$	$w_{sc1} = 1, w_{sc2} = 10$
V_1	$v_1 = 0.1$	$v_1 = 0.7$
	$f_1 = f_2 = 0.517\,\text{Hz}$	$f_1 = f_2 = 0.518\ \text{Hz}$
	$b_1 = 0.125$	$b_1 = 0.033$
	$b_2 = 0.91$	$b_2 = 0.8$
W_1	$w_1 = 1.2$	$w_1 = 1$
V_2	$v_{21} = 4, v_{22} = 0.125$	$v_{21} = 5, v_{22} = 0.167$
V_3	$v_3 = 1.286$	$v_3 = 1.135$
W_2	$P_I = 0.1$	$P_I = 0.01$
	$f_I = 0.134$	$f_I = 1$
	$w_{22} = 0.5$	$w_{22} = 0.01$
W_3	$w_3 = 0.243$	$w_3 = 0.0044$
	$f_R = 0.469$	$f_R = 1$
	$\beta = 0.1$	$\beta = 0.1$

controllers have distinct frequency-dependent characteristics within the frequency range of the torsional resonance modes of the drill-string system (see Fig. 21), which is not the case for the SoftTorque controller. This industrial controller, which only uses top drive velocity measurements, is a properly tuned active damping system (i.e., PI-control of the angular velocity), which aims at damping only the first torsional mode of the drill-string dynamics.

The resulting measured bit-mobilities are shown in Fig. 27. It can be seen that the designed controllers suppress the first and second flexibility mode in the bit-mobility. However, the third mode is only slightly damped using these controllers. Clearly, the high-gain controller ($\mathscr{H}_\infty$ (hg)) achieves more damping of the third mode than the low-gain controller ($\mathscr{H}_\infty$ (lg)). The limited amount of damping of this mode is caused by the fact that it is difficult to synthesize a controller that suppresses the third flexibility mode and at the same time satisfies the performance specifications regarding measurement noise sensitivity. The sensitivity with respect to measurement noise plays an important role in the design of controllers for the experimental setup, because the level of noise (especially on the top drive angular velocity) is relatively high. In addition, the third mode is almost unobservable in, e.g., the frequency response function from top-drive torque to top-drive velocity, see Fig. 10. Therefore, it is difficult to suppress the third torsional flexibility mode.

Remark 1 We conjecture that (e.g., torque) sensors in the drill-string can significantly improve the observability properties of such essential flexibility modes, and can hence potentially be used in a feedback strategy to improve the damping of such modes that are poorly observable in surface measurements.

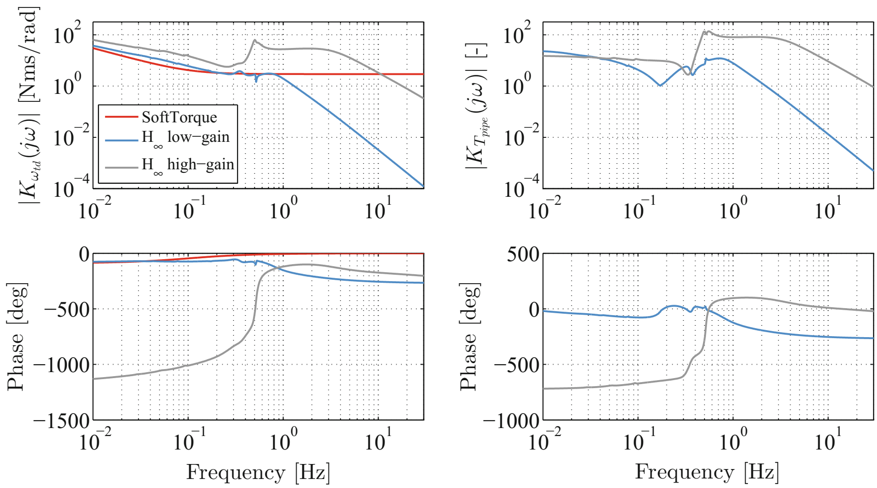

Fig. 26 Designed linear dynamic controllers (and Soft-Torque controller) for the experimental drill-string setup. Left plot is the controller that uses the top drive angular velocity, while the controller in the right plot is based on the pipe torque measurement

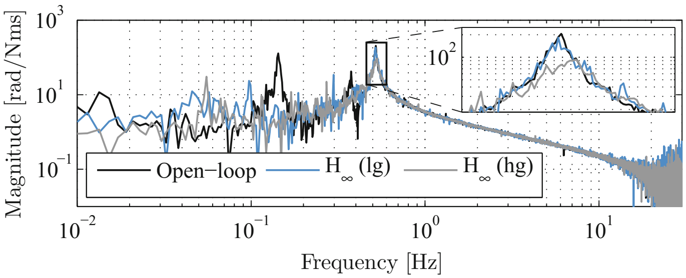

Fig. 27 Bit-mobility of the setup with two different $\mathscr{H}_\infty$-controllers

The measured response is shown in Fig. 28. First, the low-gain $\mathscr{H}_\infty$-controller is used, and after approximately 210 s, we switch to the high-gain controller. This switch is not necessary, and the desired setpoint can also be stabilized using the low-gain controller only. However, the high-gain controller has improved robustness properties (due to the improved damping of the third mode), which can be beneficial. By only using the high-gain controller in the startup scenario, it is not possible to stabilize the desired setpoint. A closer look at the experimental results with the $\mathscr{H}_\infty$-controllers shows that the low-gain controller is able to stabilize the desired setpoint of 5.5 rpm with limited control action (i.e., at least the controller acts less aggressively compared to the high-gain $\mathscr{H}_\infty$-controller). The oscillations in the bit angular velocity are still relatively large in amplitude; however, the oscillations are sufficiently damped to mitigate stick-slip vibrations. In addition, it has to be noted that, due to the presence of the roll-off filters in the controller, high-frequency (measurement) noise is not amplified

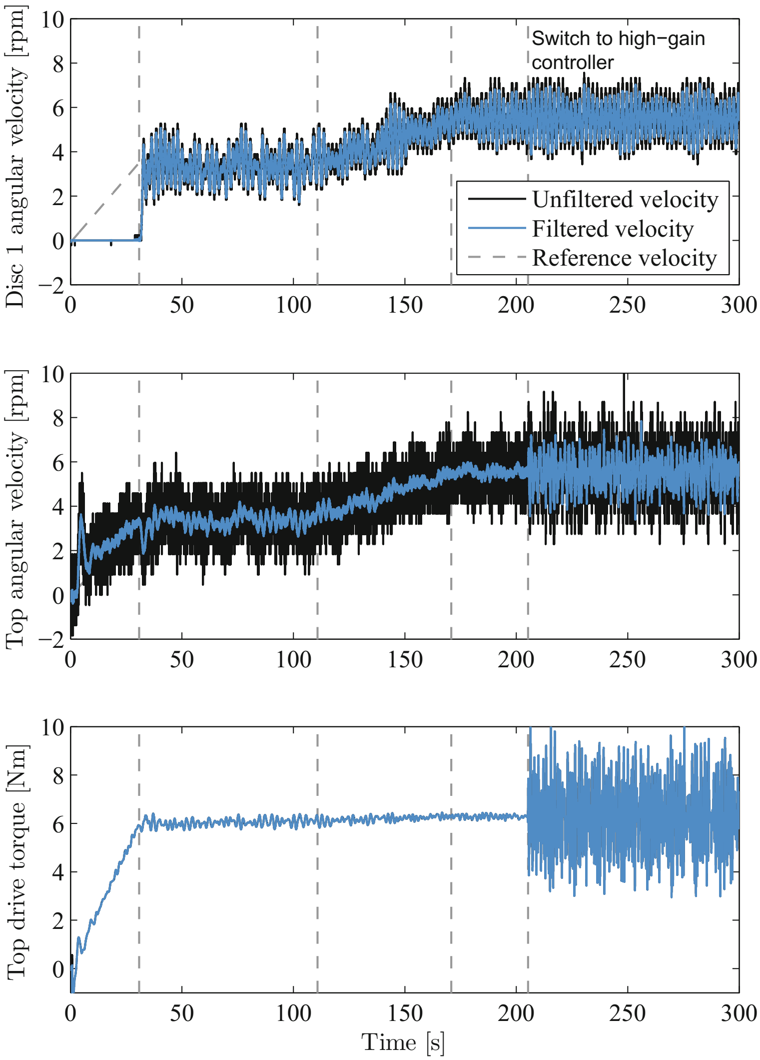

Fig. 28 Experimental result of the drill-string setup with the designed $\mathscr{H}_\infty$-controllers in the startup scenario, after approximately 210 s, the controller is switched to a high-gain $\mathscr{H}_\infty$-controller

by the controller, such that possible oscillations caused by such disturbances are avoided. The high-gain controller clearly uses more control action, which also results in more oscillations in the top drive angular velocity. The high-gain controller induces slightly larger oscillations in the bit angular velocity than those induced by the low-gain controller. The latter effect is related to the (measurement) noise sensitivity of these controllers. Still, the high-gain controller ensures a higher robustness against uncertainties in the bit-rock-interaction, as evidenced by an improved attenuation of the (third) resonance in the bit mobility, see Fig. 27.

Summarizing, with the designed $\mathscr{H}_\infty$-controllers, it is possible to stabilize a desired angular velocity of 5.5 rpm and to avoid stick-slip oscillations in a realistic scenario in which the SoftTorque controller could not avoid such oscillations.

5 Concluding Remarks

In this chapter, we have presented the design of an experimental, lab-scale drill-string setup based on a non-smooth model of a real-life drilling rig. The setup was designed to reflect multiple dominant torsional flexibility modes of the system dynamics, as field tests have shown that multiple modes can be associated with the occurrence of stick-slip oscillations. Next, we have proposed a robust control design strategy that can be used to design controllers that (1) stabilize a constant velocity setpoint, and hence avoid such stick-slip limit cycling, (2) guarantee robust stability in the presence of uncertainties in the bit-rock interaction, (3) take into account practically relevant performance specifications, and (4) guarantee robust stability and performance in the presence of multi-modal torsional drill-string dynamics. Finally, such controllers have been implemented and tested on the experimental setup, and it has been shown that these can eliminate stick-slip oscillations in realistic startup scenarios in which an industrial SoftTorque controller fails to do so.

References

1. Bresch-Pietri D, Krstic M (2014) Adaptive output-feedback for wave PDE with anti-damping—application to surface-based control of oil drilling stick-slip instability. In: Proceedings of the 53rd IEEE conference on decision and control, Los Angeles, California, U.S.A., pp 1295–1300
2. Canudas-de Wit C, Rubio F, Corchero M (2008) D-OSKIL: a new mechanism for controlling stick-slip oscillations in oil well drillstrings. IEEE Trans Control Syst Technol 16(6):1177–1191
3. Copley Controls (2015) Xenus Plus XTL-230-40. Website: http://www.copleycontrols.com/Motion/Products/Drives/Digital/xenusPlus.html
4. De Bruin JCA, Doris A, Van de Wouw N, Heemels WPMH, Nijmeijer H (2009) Control of mechanical motion systems with non-collocation of actuation and friction: a Popov criterion approach for input-to-state stability and set-valued nonlinearities. Automatica 45(2):405–415
5. Detournay E, Defourny P (1992) A phenomenological model for the drilling action of drag bits. Int J Rock Mech Mining Sci Geomech Abstracts 29(1):13–23
6. Doris A (2013) Method and system for controlling vibrations in a drilling system. Patent WO 2013(076184):A2
7. dSPACE (2015) DS1103 ppc controller board, https://www.dspace.com/en/inc/home/products/hw/singbord/ppcconbo.cfm
8. Dwars S (2015) Recent advances in soft torque rotary systems. In: SPE/IADC Drilling conference and exhibition, SPE/IADC 173037, London, United Kingdom
9. Georgii Kobold (2015) KTY-F torque motors, http://www.georgiikobold.de/en/products/Torque-Motors-KTY.b7059.php
10. Géradin M, Rixen D (1997) Mechanical vibrations: theory and application to structural dynamics, 2nd edn. Wiley, Chichester, England

11. Grauwmans R, Stulemeijer I (2009) Drilling efficiency optimization: vibration study, presentation shell exploration and production, Rijswijk, the Netherlands
12. Halsey GW, Kyllingstad A, Kylling A (1988) Torque feedback used to cure slip-stick motion. In: SPE annual technical conference and exhibition, Houston, Texas, U.S.A., SPE 18049, pp 277–282
13. Heidenhain (2015) Encoders for servo drives, pp 70–71. http://www.heidenhain.com/
14. Jansen JD, Van den Steen L (1995) Active damping of self-excited torsional vibrations in oil-well drillstrings. J Sound Vib 179(4):647–668
15. Karkoub M, Zribi M, Elchaar L, Lamont L (2010) Robust μ-synthesis controllers for suppressing stick-slip induced vibrations in oil well drill strings. Multibody Syst Dyn 23(2):191–207
16. Khalil H (2002) Nonlinear systems, 3rd edn. Prentice-Hall, Upper Saddle River
17. Khulief YA, Al-Sulaiman FA (2009) Laboratory investigation of drillstring vibrations. Proc Inst Mech Eng Part C: J Mech Eng Sci 223:2249–2262
18. Kovalyshen Y (2014) Experiments on stick-slip vibrations in drilling with drag bits. In: Proceedings of the 48th US rock mechanics geomechanics symposium, Minneapolis, Minnesota, USA
19. Kyllingstad A, Nessjøen PJ (2009) A new stick-slip prevention system. In: SPE/IADC drilling conference and exhibition, Amsterdam, Netherlands, SPE/IADC 199660
20. Lu H, Dumon J, Canudas-de Wit C (2009) Experimental study of the d-oskil mechanism for controlling the stick-slip oscillations in a drilling laboratory testbed. In: Proceedings of the IEEE multi-conference on systems and control, Saint Petersburg, Russia, pp 1551–1556
21. Meinsma G (1995) Unstable and nonproper weights in $\mathscr{H}_\infty$ control. Automatica 31(11):1655–1658
22. Mihajlović N, van Veggel AA, van de Wouw N, Nijmeijer H (2004) Analysis of friction-induced limit cycling in an experimental drill-string system. ASME J Dyn Syst Meas Control 126(4):709–720
23. Nessjøen PJ, Kyllingstad A, D'Ambrosio P, Fonseca IS, Garcia A, Levy B (2011) Field experience with an active stick-slip prevention system. In: SPE/IADC drilling conference and exhibition, SPE/IADC 139956, Amsterdam, Netherlands
24. Oomen T, van Herpen R, Quist S, van de Wal M, Bosgra O, Steinbuch M (2014) Connecting system identification and robust control for next-generation motion control of a wafer stage. IEEE Trans Control Syst Technol 22(1):102–118
25. Patil P, Teodoriu C (2013) A comparative review of modelling and controlling torsional vibrations and experimentation using laboratory setups. J Petrol Sci Eng 112:227–238
26. PCM (2015) RT2-rotating torque transducer. http://www.pcm-uk.com/transducer-torque-rt2.html
27. Perneder L, Detournay E (2013) Steady-state solutions of a propagating borehole. Int J Solids Struct 50:1226–1240
28. Printed Motor Works (2015) GN series. http://www.printedmotorworks.com/wp-content/uploads/GN-Series-Overview.pdf
29. Reimers N (2014) Mitigation of torsional vibrations and stick-slip induced by aggressive, energy efficient drill-bits. In: Detournay E, Denoël V, van de Wouw N, Zhou Y (eds) Third international colloquium on nonlinear dynamics and control of deep drilling systems, Minneapolis, Minnesota, USA, pp 9–14
30. Richard T, Germay C, Detournay E (2007) A simplified model to explore the root cause of stick-slip vibrations in drilling systems with drag bits. J Sound Vib 305(3):432–456
31. Serrarens AFA, Van De Molengraft MJG, Kok JJ, Van Den Steen L (1998) $\mathscr{H}_\infty$ control for suppressing stick-slip in oil well drillstrings. IEEE Control Syst Mag 18(2):19–30
32. Sick (2015) DFS60A incremental encoder. http://www.sick.com/
33. Sieb & Meyer (2015) SD2S drive amplifier. http://www.sieb-meyer.de/
34. Skogestad S, Postlethwaite I (2005) Multivariable feedback control, 2nd edn. Wiley
35. Tucker RW, Wang C (1999) On the effective control of torsional vibrations in drilling systems. J Sound Vib 224(1):101–122

36. Vlajic N, Balachandran B (2014) Nonlinear and delay effects in drilling mechanics. In: Detournay E, Denoël V, van de Wouw N, Zhou Y (eds) Third international colloquium on nonlinear dynamics and control of deep drilling systems, Minneapolis, Minnesota, USA, pp 51–66
37. Vromen T (2015) Control of stick-slip vibrations in drilling systems. PhD thesis, Eindhoven University of Technology, Eindhoven, The Netherlands
38. Vromen T, Dai CH, van de Wouw N, Oomen T, Astrid P, Nijmeijer H (2015) Robust output-feedback control to eliminate stick-slip oscillations in drill-string systems. In: 2nd IFAC workshop on automatic control in offshore oil and gas production, Florianopolis, Brazil, pp 272–277
39. Vromen T, van de Wouw N, Doris A, Astrid P, Nijmeijer H (2017) Nonlinear output-feedback control of torsional vibrations in drilling systems. Int J Robust Nonlinear Control. https://doi.org/10.1002/rnc.3759
40. Wiercigroch M, Pavlovskaia E, Vaziri V, Kapitaniak M (2014) Resonance enhanced drilling: modelling, experiments and design. In: Detournay E, Denoël V, van de Wouw N, Zhou Y (eds) Third international colloquium on nonlinear dynamics and control of deep drilling systems, Minneapolis, Minnesota, USA, pp 1–7
41. Zhou K, Doyle J, Glover K (1996) Robust and optimal control. Prentice Hall, Upper Saddle River